


**Electronic Band Structure of Iridates**

Journal:	<i>Materials Horizons</i>
Manuscript ID	MH-REV-01-2021-000063.R1
Article Type:	Review Article
Date Submitted by the Author:	20-Mar-2021
Complete List of Authors:	Dhingra, Archit; University of Nebraska-Lincoln, Physics and Astronomy Komesu, Takashi; University of Nebraska-Lincoln, Physics and Astronomy Kumar, Shiv Kumar; Hiroshima University, Hiroshima Synchrotron Radiation Center Shimada, Kenya; Hiroshima University, Hiroshima Synchrotron Radiation Center Zhang, Le; University of Nebraska-Lincoln, Physics and Astronomy Hong, Xia; University of Nebraska-Lincoln, Physics and Astronomy Dowben, Peter; University of Nebraska-Lincoln, Physics and Astronomy

## ARTICLE

## Electronic Band Structure of Iridates

Archit Dhingra,<sup>\*a</sup> Takashi Komesu,<sup>a</sup> Shiv Kumar,<sup>b</sup> Kenya Shimada,<sup>b</sup> Le Zhang,<sup>a</sup> Xia Hong<sup>a</sup> and Peter A. Dowben<sup>a</sup>

Received 00th January 20xx,  
Accepted 00th January 20xx

DOI: 10.1039/x0xx00000x

Here, an attempt has been made to compare the electronic structure of many of the 5d iridates, making some effort to note commonalities in their band structure, as well as differences, as revealed by various experimental studies, as well as the first-principles band structure calculations, although relying principally upon angle-resolved photoemission spectroscopy (ARPES). This brings to focus the fact that the electronic structure and magnetic properties of the high-Z 5d transition iridate depend on the interplay of strong electron correlation, strong (relativistic) spin-orbit coupling, lattice distortion, as well as the dimensionality of the system. For example, several iridates (iridium oxides), such as SrIrO<sub>3</sub>, exhibit a metal-insulator transition that is dimensionality dependent, which in the thin film limit, resembles bulk Sr<sub>2</sub>IrO<sub>4</sub>.

## Introduction

Compared with their 3d counterparts, the 5d transition metal oxides (TMOs) possess several distinct properties: (i) the tunable electron correlation expected of more extended *d*-orbitals; (ii) the stronger spin-orbit coupling (SOC) typical of high-Z elements,<sup>1–4</sup> which can split the otherwise degenerate valence and conduction bands into bands that are distinguished by angular momentum, namely  $J_{\text{eff}} = 1/2$  and  $J_{\text{eff}} = 3/2$  bands (see ref. 3 for detailed representation of these states in Dirac notation). The splitting between the quartet of states (corresponding to  $J_{\text{eff}} = 3/2$ ) and the doublet (corresponding to  $J_{\text{eff}} = 1/2$ ) may be large. The comparable electron correlation and SOC, in conjunction with the presence of crystal field splitting and the potential of inter-site hopping, can yield an even richer spectrum of electronic and magnetic behaviors in these materials in comparison with 3d TMOs.<sup>1,5</sup> Hund's rule coupling<sup>6</sup> cannot lead to a complete description of the physical properties of these systems, by itself, and thus differs from many of the 4d TMOs, where Hund's rules are a dominant factor.<sup>7</sup>

Due to the narrowing of bandwidth ( $W$ ), as a result of structural distortions<sup>2</sup> and reductions in dimensionality, electronic correlations may be enhanced to an extent that the compounds become insulating.<sup>3</sup> In spite of an unpaired electron (an odd number of valence electrons). In the context of the Hubbard model, some iridates exhibit Mott type metal-insulator transition (MIT) driven by electron correlation and dimensionality, i.e. Mott physics, can be systematically examined in the 5d TMOs due to the presence of competing energy scales of bandwidth ( $W$ ) and correlation, i.e. on-site

Coulomb interaction ( $U$ ).<sup>8</sup> Electron correlation is of interest because it can play a big role in the vicinity of the MIT leading to enhanced effective conducting carrier masses.<sup>8–11</sup> In the case of iridates, there is clearly an interplay between SOC, structural distortions, Coulomb correlations, and bandwidth.<sup>1–3</sup> Correlation interactions enhance spin-orbital polarization to leave the  $J_{\text{eff}} = 1/2$  band half-filled and split by a Hubbard  $U$  at the Fermi level, while the  $J_{\text{eff}} = 3/2$  exhibits the higher binding energy. Generally, the larger occupied  $J$  component has the smaller binding energy, and thus, if occupied, is closer to the Fermi level than the smaller  $J$  component, but this expectation does not hold true for the iridates. In other words, for the iridates, it is more typical to see that  $J_{\text{eff}} = 3/2$  has a larger binding energy than  $J_{\text{eff}} = 1/2$ .<sup>1–3</sup> In the context of the Hubbard model, which depicts the ground state of such systems by considering the on-site Coulomb interaction ( $U$ ) and the bandwidth ( $W$ ), a key issue for the iridates is whether  $W \ll U$  leads to an insulating state (called Mott insulator) or  $W \gtrsim U$  yields the more expected metallic state, because of the odd number of d electrons in the iridates.

The presence of physical properties, such as SOC, film thickness dependent metallicity, etc., and their delicate interplay, can lead to a competition between different ground states.<sup>1–4,12–15</sup> The 5d iridates have been predicted to exhibit a variety of phenomena:<sup>7,13,14,16</sup> including high  $T_c$  superconductivity,<sup>17</sup> quantum spin Hall effect,<sup>18</sup> topological insulators,<sup>19–21</sup> correlated topological insulators with large gaps enhanced by Mott physics (i.e. the metal to nonmetal transition),<sup>18,22–24</sup> topological semimetals,<sup>25</sup> Weyl semimetals with Fermi arcs,<sup>26,27</sup> axion insulators (magnetic topological insulators) with strong magnetoelectric coupling,<sup>28</sup> Kitaev modes,<sup>29,30</sup> and 3D spin liquids with Fermionic spinons.<sup>31</sup> On the experimental side a wide range of intriguing phenomena have been observed, such as lattice-driven magnetoresistivity,<sup>32</sup> giant magnetoelectric effect,<sup>33</sup> a spin liquid phase in a hyperkagome structure,<sup>34</sup>  $J_{\text{eff}} = 1/2$  Mott insulator state,<sup>35–37</sup> a zig-zag magnetic structure,<sup>38,39</sup> and unusual orbital magnetism

<sup>a</sup> Department of Physics and Astronomy, Nebraska Center for Materials and Nanoscience, Theodore Jorgensen Hall, 855 N 16th, University of Nebraska, P.O. Box 880299, Lincoln, Nebraska 68588-0299, U.S.A.

<sup>b</sup> Hiroshima Synchrotron Radiation Center (HSOR), Hiroshima University, Higashi-Hiroshima 739-0046, Japan

(it is unusual as it is driven by a strong spin-orbit coupling).<sup>40</sup> Some iridates may be magnetic insulators bearing exotic magnetic and electronic properties.<sup>41–44</sup>

Overall, the band structure is key to understanding many of the unusual properties of the iridates. Beginning with  $\text{IrO}_2$ , the electronic structure of many iridate systems can be understood by realizing that each  $\text{Ir}^{4+}$  is coordinated by six  $\text{O}^{2-}$  forming an octahedron. Even though the octahedral symmetry of the iridates is frequently distorted, the  $\text{Ir } 5d$  orbitals are split up into what is generally considered a  $t_{2g}$  triplet and an  $e_g$  doublet. The crystal field splitting is such that the  $e_g$  band is typically about 2 eV higher than the Fermi level while the  $\text{Ir } t_{2g}$  have the major contribution to the bands near the Fermi level along with some mixing with the  $\text{O } 2p$  states. This then tends to dominate the electronic structure of the iridates. In terms of band structure, some well-studied iridates beyond  $\text{IrO}_2$  are: (a) the pyrochlore iridates of the form  $\text{A}_2\text{Ir}_2\text{O}_7$ , including  $\text{Bi}_2\text{Ir}_2\text{O}_7$ ; (b)  $\text{BaIrO}_3$ ; (c)  $\text{Ba}_2\text{IrO}_4$ ; (d)  $\text{Sr}_{n+1}\text{Ir}_n\text{O}_{3n+1}$  ( $n = 1, 2, \infty$ ); (e) alkali metal iridates of the form  $\text{T}_2\text{IrO}_3$ ; and (f) calcium iridates, i.e.,  $\text{CaIrO}_3$  and  $\text{Ca}_5\text{Ir}_3\text{O}_{12}$ . Although the formal charge on Ir on all these iridates is the same, the many band structure studies provide insights into the variability of the  $\text{IrO}_2$  building block,<sup>13,45</sup> affecting metallicity and correlation effects.

We note that density functional theory (DFT), in the framework of Perdew–Burke–Ernzerhof (PBE)<sup>13,46,47</sup> and other methodologies, frequently underestimates the band gap for semiconductors or insulators as is in fact expected,<sup>48–52</sup> so exact agreement between theory and experiment should not be expected, especially for the unoccupied states. We note that in general, here in this review, binding energies are in terms of  $E - E_F$ , thus the occupied states have negative binding energies, with the exception being Figure 11.

$\text{IrO}_2$  is the foundational iridate. This system has the distorted quasi-octahedral configuration of  $\text{IrO}_6$ , common to many iridates, as its basic structural component. Some of the basic characteristics of the band structure of  $\text{IrO}_2$  also appear in the band structure of the other iridates. This makes  $\text{IrO}_2$  a good starting point for a general discussion about the band structure of iridates. Not surprisingly, this binary system has been a subject of several theoretical<sup>13,45,53</sup> and experimental<sup>54–59</sup> studies of electronic properties.

In one recent study carried out by Xu *et al.*,<sup>54</sup>  $\text{IrO}_2$  single crystals were found to crystallize into the rutile-type structure with lattice constants  $a$ ,  $b$  and  $c$  being 4.498 Å, 4.498 Å and 3.154 Å, respectively, with space group  $P4_2/mnm$ . The experimental band structure was obtained not just along the surface Brillouin zone, but included a determination of the bulk band structure, across the bulk Brillouin zone, as summarized in Figure 1a, was obtained using photon energy dependent angle-resolved photoemission. Figure 1b depicts the calculated structure of the  $\text{IrO}_2$  Fermi surface, which was obtained using the Vienna *ab initio* Simulation Package (VASP) (see ref. 54 for further computational details). Figures 1c–1e depict the bulk  $\text{IrO}_2$  Fermi surfaces, calculated at different values of  $k_z$  ( $=0, \pi/2d$ , and  $\pi/d$ , respectively). The experimental bulk Fermi surfaces obtained using photon energy dependent ARPES corresponding to  $k_z = 0$  (a photon energy of 122 eV),  $k_z = \pi/2d$  (138 eV) and  $k_z = \pi/d$  (164 eV) are shown in Figures 1f–1h, respectively, demonstrating good agreement between theory and experiment. Furthermore, band dispersions measured along high symmetry directions,  $\text{Z}\Gamma\text{Z}$  and  $\text{AMA}$ , are shown in

## The basic iridate: $\text{IrO}_2$

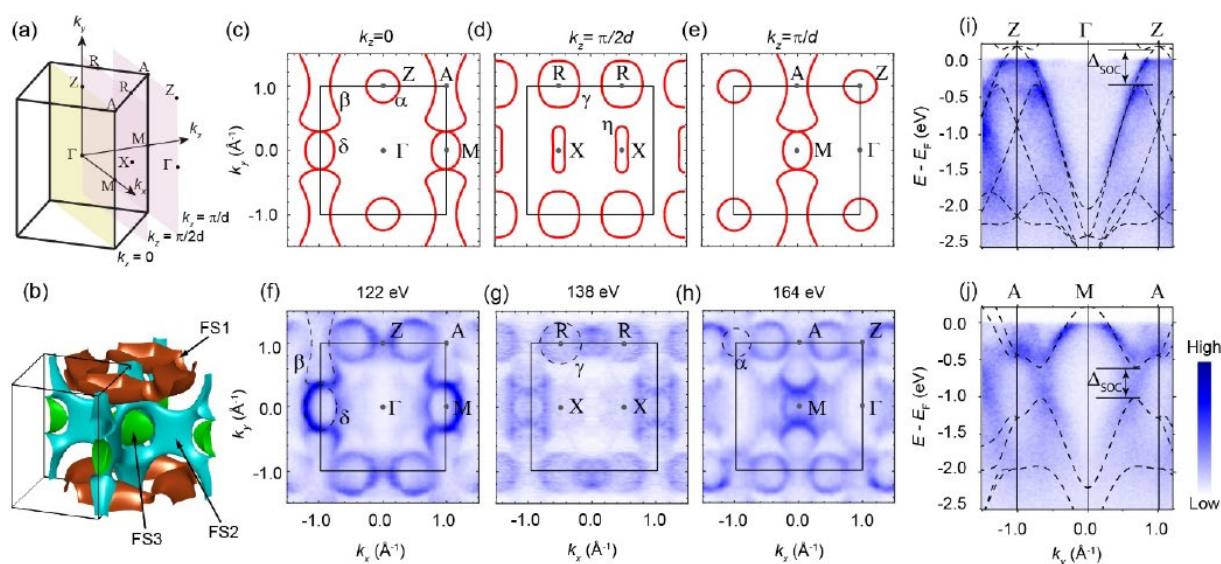


**Figure 1.** (a) The 3D BZ of  $\text{IrO}_2$ , with the indication of planes at  $k_z = 0$ ,  $k_z = \pi/2d$ , and  $k_z = \pi/d$ . (b) Calculated Fermi surface structure of  $\text{IrO}_2$ . (c–e) Calculated bulk Fermi surfaces at  $k_z = 0$ ,  $k_z = \pi/2d$  and  $k_z = \pi/d$ , respectively. (f–h) Photoemission intensity map in  $k_x$ – $k_y$  plane obtained at different photon energies. (i) Band dispersion measured along  $\text{Z}\Gamma\text{Z}$ . (j) Band dispersion measured along  $\text{AMA}$  direction. The data were collected at 10 K, and calculated bulk band structure (dashed lines) are overlaid for comparison. Reprinted figure with permission from ref. 54. Copyright (2019) by the American Physical Society.

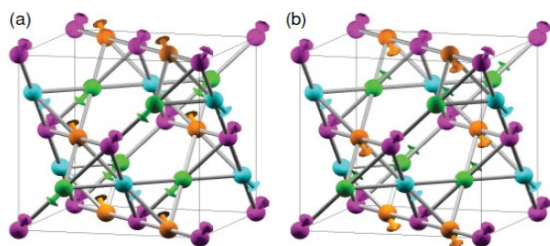


**Figure 2.** The crystal structure of pyrochlore iridates showing Ir atoms (green) at the corner of the tetrahedral network along with their two possible magnetic configurations: (a) The predicted, all-in/all-out magnetic order configuration for iridates; and (b) the alternative 2-in/2-out configuration. Reprinted figure with permission from ref. 26. Copyright (2011) by the American Physical Society.

Figures 1i and 1j, respectively. All the data was collected at 10 K, leading to higher resolution in the experiment through suppression of phonon broadening. Although not noted by the authors, the deviation from the expected band dispersion in Figure 1j does suggest an increase in effective mass in the region of the Fermi level. This mass enhancement might be due to electron-phonon coupling, as has been seen for metal surfaces<sup>60</sup> like Be(0001),<sup>61</sup> Cu(111),<sup>62,63</sup> Ag(111),<sup>62,63</sup> Au(111),<sup>63</sup> and NbSe<sub>2</sub>.<sup>64</sup> Such electron-phonon coupling leading to mass enhancement, while not commonly pursued for oxides, could be indicative of a non-trivial Eliashberg function.

Overall, the correlation effects in IrO<sub>2</sub> are found to be weak as there is agreement between the band structure from theory and experiment even in a large energy range, without the inclusion of a large correlation energy in the calculated band structure. This is evident in the lack of a serious discrepancy when the calculated bulk band structures are superimposed on top of the experimental data as shown in Figure 1. Additionally, the presence of strong SOC effect is manifested in the band splitting, as evident in the Figures 1i and 1j. This leads to a gap in the occupied band structure near the top of the valence band, but not at the top of the valence band. Therefore, the combination of weak correlation combined with strong SOC suggest that the impact of SOC-enhanced correlation on metallic IrO<sub>2</sub> is negligible.<sup>54</sup> The observed band splitting because of the strong SOC effect is key as even though IrO<sub>2</sub> is isostructural with RuO<sub>2</sub>, their electronic structures are considerably different due to weaker inherent SOC in the latter.<sup>54,65</sup>

### Pyrochlore Iridates (general formula: A<sub>2</sub>Ir<sub>2</sub>O<sub>7</sub>) and Bi<sub>2</sub>Ir<sub>2</sub>O<sub>7</sub>

Studies of the pyrochlore iridates, with the general formula A<sub>2</sub>Ir<sub>2</sub>O<sub>7</sub> (where A = a Lanthanide element or Yttrium), have shown magnetic ordering (which violates time-reversal symmetry).<sup>66,67</sup> Violation of time-reversal symmetry, implied by the existence of magnetic ordering, suggests that these iridates cannot exist as topological insulators since presence of time-reversal symmetry is a prerequisite. In this regard, a theoretical study (B.-J. Yang *et al.*<sup>19</sup>) indicated that these A<sub>2</sub>Ir<sub>2</sub>O<sub>7</sub> systems could exist as topological insulators although was still found to be inconsistent with the experiment. X. Wan *et al.*<sup>26</sup> predicted

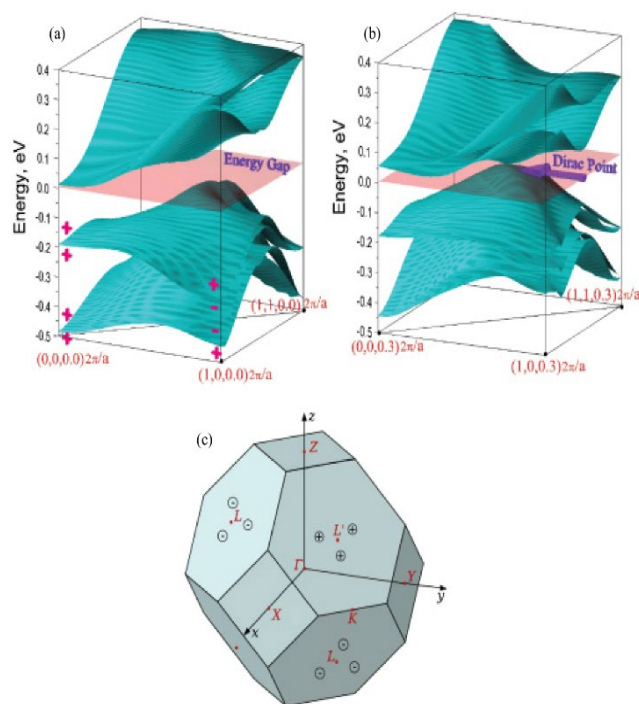


**Figure 3.** LSDA + *U* + SO band structure calculations (for *U* = 1.5 eV) showing semimetallic nature of Y<sub>2</sub>Ir<sub>2</sub>O<sub>7</sub>. (a) The calculated energy bands in the plane *k<sub>x</sub>* = 0 along with depiction of band parities. (b) The energy bands in the plane *k<sub>y</sub>* = 0 along with depiction of band parities. The lighter shaded plane marks the Fermi level. (c) The nine Weyl point locations within the 3-D Brillouin zone are indicated by circled + and - signs. The binding energies are in terms of E-E<sub>F</sub>, thus the occupied states have negative binding energies. Reprinted figure with permission from ref. 26. Copyright (2011) by the American Physical Society.

that some of the pyrochlore iridates can be found to exist in a phase known as topological semimetal based on local spin density approximation (LSDA) + *U* + SO calculations, where, SO stands for spin-orbit coupling parameter, and *U* is the correlation strength (or the interaction parameter). In these A<sub>2</sub>Ir<sub>2</sub>O<sub>7</sub> systems, both, A and Ir atoms are found to be located on a network of corner-sharing tetrahedra.<sup>68,69</sup> In other words, these systems comprise of four Ir atoms inside each unit cell forming a tetrahedral network, as illustrated in Figure 2.

Experiments<sup>70–72</sup> have successfully shown that there is an evolution of ground state properties, with increments in the radius of the A ion for a given A<sub>2</sub>Ir<sub>2</sub>O<sub>7</sub> system. Since radii of A ions are believed to tune the electronic correlation, this implies that the electronic properties of such systems may be altered considerably as is evident from the observed variation of optical conductivity spectra within a series of A<sub>2</sub>Ir<sub>2</sub>O<sub>7</sub> iridates.<sup>73</sup> Therefore, the pyrochlore iridate with A = Pr manifests semimetallic behavior,<sup>74</sup> whereas for A = Y the iridate is an insulator at low temperatures.<sup>70</sup> A similar transition effect is seen when these iridates are subject to varying external pressure, which underscores the importance of effective correlation in MIT.<sup>75</sup> The role of SOC, with respect to A<sub>2</sub>Ir<sub>2</sub>O<sub>7</sub>, is to lift degeneracies of these t<sub>2g</sub> states while producing a quadruplet with *J<sub>eff</sub>* = 3/2 and a higher-energy Kramers doublet with *J<sub>eff</sub>* = 1/2,<sup>35</sup> as was indicated at the outset to be a common feature for the iridates. Besides, the interaction between the local moments (due to rare-earth *f* electrons) and the itinerant

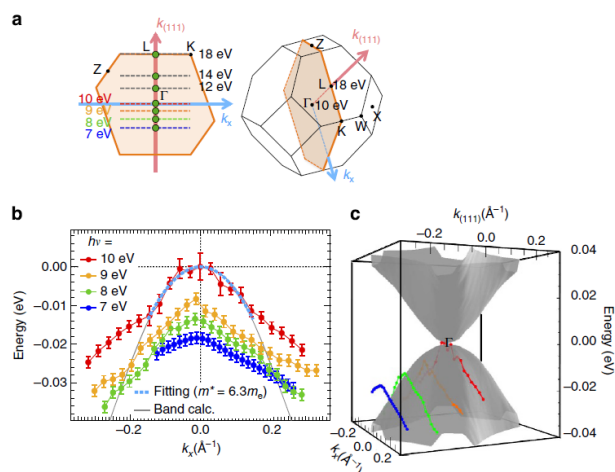


**Figure 4.** The ARPES spectra of  $\text{Pr}_2\text{Ir}_2\text{O}_7$ . (a) The  $\text{Pr}_2\text{Ir}_2\text{O}_7$  Brillouin zone, showing roughly momentum cuts for which the experimental ARPES spectra were collected. Iso-energy band mappings were taken at photon energies between  $h\nu = 10$  and  $18$  eV cross the  $\Gamma$  and L points in the first Brillouin zone. (b) The experimental energy dispersion plots along the  $k_x$  direction measured at  $h\nu = 7, 8, 9$  and  $10$  eV, roughly corresponding momentum cuts indicated in (a) by dashed coloured lines. The data close to  $E_F$  is fitted using a parabolic function,  $\epsilon(k) \propto k^2$  (light-blue dotted curve in (b)). Estimated effective mass at  $\Gamma$ ,  $m_{\text{eff}} = 6.3m_0$ , agrees with the calculations. (c) The band dispersion obtained by first-principles in the calculated band dispersion in the  $k_x - k_{(111)}$  sheet (grey), indicated by the orange in (a), superimposed on the experimental iso-energy  $\epsilon(k)$  versus  $k_x$  plots. The binding energies are in terms of  $E - E_F$ , thus the occupied states have negative binding energies. Reproduced from ref. 74. CC BY 4.0

Ir 5d electrons is crucial as the precise behaviour of electronic states is contingent on the magnetic configuration.<sup>76–82</sup>

Based on the results of LSDA +  $U$  + SO band structure calculations (Figure 3), it has been proposed that  $\text{Y}_2\text{Ir}_2\text{O}_7$  (and possibly other  $\text{A}_2\text{Ir}_2\text{O}_7$  pyrochlore iridates, with  $A = \text{Eu}, \text{Sm}$ , and  $\text{Nd}$ ) is a Weyl semimetal, with a band structure in proximity to a Mott insulating state,<sup>26,83</sup> and with the potential for magnetic ordering. This connection between magnetic properties and insulating behaviour is found to be consistent with experiment.<sup>66,67</sup> Additionally, the tendency towards semimetal behaviour is found to be consistent with trend towards a metallic phase on lowering the correlation strength, as in the case where  $A = \text{Pr}$  (Figure 4).<sup>70–72,74</sup> Recently, charge transport measurements on hole-doped pyrochlore iridates of Pr, Nd, and Eu were reported, and it was found that these systems can show enhanced thermopower with values as high as  $45 \mu\text{V}/\text{K}$ .<sup>84</sup> In addition to showing considerable thermopower peak, this study by Kaneko *et al.*<sup>84</sup> also suggests that topologically protected character of bands is maintained even in strongly correlated systems near the Mott transition. This<sup>84</sup> further implies that the creation of Weyl semimetallic phase can be achieved in this class of iridates on the verge of filling-controlled Mott transition.

The  $\text{Bi}_2\text{Ir}_2\text{O}_7$  (Bi-227) iridate has the same formula as other pyrochlore iridates but lacks a magnetic moment on the  $\text{Bi}^{3+}$  ions. This makes  $\text{Bi}_2\text{Ir}_2\text{O}_7$  unique, as the lack of magnetic moment helps in the distinction between the physics originating from the Ir subsystem versus the properties originating due to the other underlying reasons.<sup>4</sup> Qi *et al.*<sup>12</sup> carried out an extensive magnetic susceptibility, specific heat and transport measurements as well as performed band structure calculations for single-crystal  $\text{Bi}_2\text{Ir}_2\text{O}_7$  where substitution of the  $\text{Bi}^{3+}$  ion for

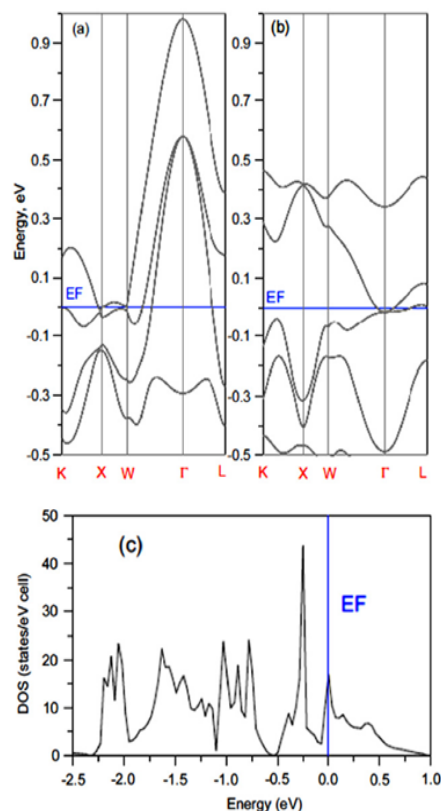


**Figure 5.** The LDA + SOC density functional theory calculations of (a) the band structure of  $\text{Bi}_2\text{Ir}_2\text{O}_7$ ; (b) the band structure of  $\text{Y}_2\text{Ir}_2\text{O}_7$  (for comparison); and (c) density of states for  $\text{Bi}_2\text{Ir}_2\text{O}_7$ . The  $J_{\text{eff}} = 1/2$  bands extend from a binding energy of  $-0.5$  to  $1.0$  eV, with the binding energy in terms of  $E - E_F$ , so the occupied states have negative binding energies.<sup>12</sup> © IOP Publishing. Reproduced with permission. All rights reserved.

the rare earth ion considerably enhances the hybridization between the Bi 6s/6p and Ir 5d electrons. This enhanced hybridization is found to be stronger than the SOC and  $U$  terms which, in turn, renders the ground state of the material metallic.<sup>85</sup> Yet  $\text{Bi}_2\text{Ir}_2\text{O}_7$ , and  $\text{Y}_2\text{Ir}_2\text{O}_7$  were found to have very different band structures in non-magnetic, nonspin-resolved, “LDA + SOC” DFT calculations,<sup>12</sup> as shown in Figure 5.

Even though  $\text{Bi}_2\text{Ir}_2\text{O}_7$  and  $\text{Y}_2\text{Ir}_2\text{O}_7$  have similar lattice parameters and Ir–O–Ir bond angles,  $\text{Bi}_2\text{Ir}_2\text{O}_7$  happens to have the wider  $J_{\text{eff}} = 1/2$  bandwidth of the two pyrochlore iridates as can be seen in Figure 5a and Figure 5b.<sup>12</sup> The  $J_{\text{eff}} = 1/2$  bands extend from  $-0.5$  to  $1.0$  eV for  $\text{Bi}_2\text{Ir}_2\text{O}_7$  but not for  $\text{Y}_2\text{Ir}_2\text{O}_7$ .<sup>12</sup> Interestingly, the Fermi level,  $E_F$ , placement for of  $\text{Bi}_2\text{Ir}_2\text{O}_7$  is near one of the sharp peaks in the DOS, as shown in Figure 5c. The reason behind the peak in the DOS at the Fermi level is mainly derived from the maxima and minima in the band structure around the K, X and W points.

Based on the experimental and theoretical studies, carried out independently by Wang *et al.*<sup>4</sup> and Qi *et al.*,<sup>12</sup> it was concluded that  $\text{Bi}_2\text{Ir}_2\text{O}_7$  is metallic (for the variation of  $U$  between  $0.5$  and  $1.5$  eV), as is evident in the Fermi level band crossings, as seen in Figure 5a. Depending on the competing SOC and  $U$  interactions, in this iridate system, the existence of either a non-Fermi liquid state with magnetic instability or strong exchange-enhanced paramagnetic state is indicated.<sup>12</sup>

## The high-symmetry iridate: Ba<sub>2</sub>IrO<sub>4</sub>

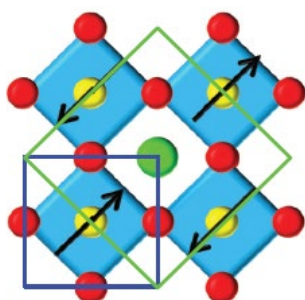


**Figure 6.** The projection of Ba<sub>2</sub>IrO<sub>4</sub> structure on the *ab* plane (red = O; green = Ba; and yellow = Ir). The apical oxygen atoms are not shown. The arrows illustrate Ir spin arrangement in the AFM phase, while blue and green squares represent the primitive and magnetic unit cells, respectively. Reproduced from ref. 7. CC BY 3.0

Ba<sub>2</sub>IrO<sub>4</sub> does not exhibit rotational distortion of the iridate octahedra (as indicated in Figure 6), even though the Ba has a large radius. The presence of an undistorted IrO<sub>2</sub> square lattice distinguishes Ba<sub>2</sub>IrO<sub>4</sub> from many other iridates. This means that Ba<sub>2</sub>IrO<sub>4</sub> offers the possibility of studying the electronic structure of an iridate with an undistorted IrO<sub>2</sub> square lattice.<sup>7</sup> The surface Brillouin zone shown in Figure 7a (the blue square) corresponding to the crystallographic unit cell of Figure 6.<sup>86</sup>

Angle-resolved photoemission spectroscopy (ARPES) on Ba<sub>2</sub>IrO<sub>4</sub> (Ba-214) was combined with first-principles “LDA + *U* + SO” DFT calculations as well as a tight-binding (TB) calculations with a minimum set of orbitals to analyse the experimental data.<sup>7</sup> An ARPES constant energy map of Ba<sub>2</sub>IrO<sub>4</sub> measured near the top of the valence band (at  $E = -0.1$  eV) has been presented in Figure 7a, suggests a small band gap insulator, consistent with theory.<sup>7</sup> Experimental  $E$  versus  $k_{||}$  dispersion along high-symmetry lines (marked as (b), (c) and (d) in Figure 7a) has been represented in Figure 7b, Figure 7c, and Figure 7d. Along  $M\Gamma M$  line of the Brillouin zone, a prominent band with a maximum at the  $M$  point, as seen in in Figure 7b, gives rise to

the  $\alpha$  contour indicated in the iso-energy plot, as in Figure 7a. This band corresponds to Ir states with  $J_{\text{eff}} = 3/2$ . In Figure 7c, a second band is shown with a maximum at the Brillouin zone  $X$  point generating the  $\beta$  contour indicated in the iso-energy plot of Figure 7a. In Figure 7d, the maxima of this band along  $X\Gamma X$  line, of the Brillouin zone, can be seen more clearly along with a dispersive feature, which is associated with  $\alpha^*$  contour, at  $\Gamma$ . The  $k_x$  versus  $k_z$  iso-energy map for  $E = -0.4$  eV and  $k_y = \pi/a$ , which is extracted from ARPES measurements with photon energies ranging between 95–162 eV show little or no dispersion, as seen in Figure 7e. Barring slight intensity variations with photon energies, this data is independent of  $k_z$ , and thus does not provide an indication (nor an insight) into the bulk band structure, as has been observed with orthorhombic SrIrO<sub>3</sub>(001) thin films discussed below.

The all-electron LDA + *U* + SO and tight-binding calculations on Ba<sub>2</sub>IrO<sub>4</sub> agree with the ARPES<sup>7,87</sup> (Figure 7), and tend to indicate the existence of an energy gap well above  $T_N$  ( $= 230$  K),<sup>7</sup> favouring a Mott insulator scenario (an insulating gap due to Coulombic repulsion) as opposed to a Slater scenario where the insulating gap is due to the long-range magnetic ordering.<sup>7</sup> Interestingly, this iridate resembles the band structure of SrIrO<sub>3</sub>, as noted elsewhere,<sup>88</sup> although without the bands that cross the Fermi level, as does occur for SrIrO<sub>3</sub>. So Ba<sub>2</sub>IrO<sub>4</sub> may be expected to better resemble SrIrO<sub>3</sub> in the thin film limit, when SrIrO<sub>3</sub> goes insulating or nonmetallic.

## BaIrO<sub>3</sub>

Magnetic susceptibility measurements on polycrystalline single-phase barium iridate (BaIrO<sub>3</sub>) samples have tended to indicate the presence of weak ferromagnetism with a Curie temperature  $T_c \sim 180$  K.<sup>89,90</sup> Here, role of oxygen vacancies cannot be ignored as for other oxides, like TiO<sub>2-x</sub>, oxygen vacancies are key to the ferromagnetism.<sup>91–93</sup> Additionally, analysis of electrical resistivity, magnetization, and optical conductivity

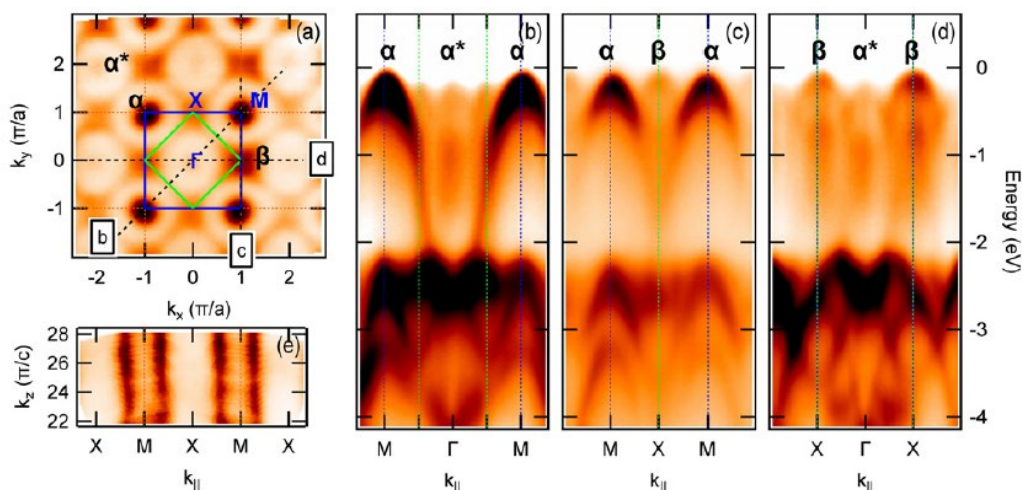


**Figure 7.** (a) An ARPES  $k_x$  versus  $k_y$  constant energy (CE) map of Ba<sub>2</sub>IrO<sub>4</sub> measured at  $E = -0.1$  eV with  $h\nu = 155$  eV and  $T = 130$  K. (b)–(d)  $E$  versus  $k_{||}$  dispersion along high-symmetry lines marked as (b), (c) and (d) in (a). Blue and green vertical lines indicate boundaries of (1x1) and the  $c(2x2)$  Brillouin zones. (e) The ARPES  $k_x$  versus  $k_z$  iso-energy or CE map for  $E = -0.4$  eV and  $k_y = \pi/a$ , extracted from scans with photon energies ranging between 95–162 eV and the assumption that inner potential,  $V_0$ , is 10 eV. Furthermore, the darkest features correspond to the largest intensity. The binding energies are in terms of  $E-E_f$ ; thus, the occupied valence band states have negative binding energies. Reproduced from ref. 7. CC BY 3.0

measurements carried out by Cao *et al.*<sup>41</sup> suggested only a small ordered spin moment on Ir ( $\sim 0.03 \mu_B/\text{Ir}$ ). The origin of this small Ir spin moment can be explained if spin polarization is the result of some spin canting as opposed to a fully compensated local moment antiferromagnetic spin configuration.<sup>90</sup>

Interestingly, magnetic susceptibility of  $\text{BaIrO}_3$  is largely insensitive to temperature above  $\sim 180 \text{ K}$ ,<sup>89,90</sup> which could imply that  $\text{BaIrO}_3$  should be a metal above  $\sim 180 \text{ K}$ . Nevertheless, electrical resistivity was observed to be independent of temperature above  $175 \text{ K}$  along the *c*-axis, whereas resistivity was found to gradually increase with a decrease in temperature along the *ab*-plane.<sup>41</sup> While such results might suggest that  $\text{BaIrO}_3$  does not appear to be a metal, anisotropic metallic character is not out of the question. Analogous to the layered compound  $\text{Sr}_6\text{V}_9\text{S}_{22}\text{O}_2$  above  $\sim 20 \text{ K}$ ,<sup>94,95</sup> a weakly localized 2-D metal could exhibit a slow-logarithmic increase in its electrical resistivity with decreasing temperature. Experimental studies have indicated that  $\text{BaIrO}_3$  may open a small charge density wave gap or pseudo-gap of  $25 \text{ meV}$  or less at low temperatures.<sup>43,96</sup> A charge density wave gap or pseudo-gap does not really negate previous theoretical studies that suggested  $\text{BaIrO}_3$  is a metallic system.<sup>97,98</sup> The possible discrepancy between experiments and initial theoretical studies is partly resolved by Ju *et al.*<sup>99</sup> In their studies, Ju *et al.*,<sup>99</sup> obtained the band structures for  $\text{BaIrO}_3$  using the LDA (Figure 8a), LSDA + *U* (Figure 8b), LSDA + SOC (Figure 8c), and LSDA +

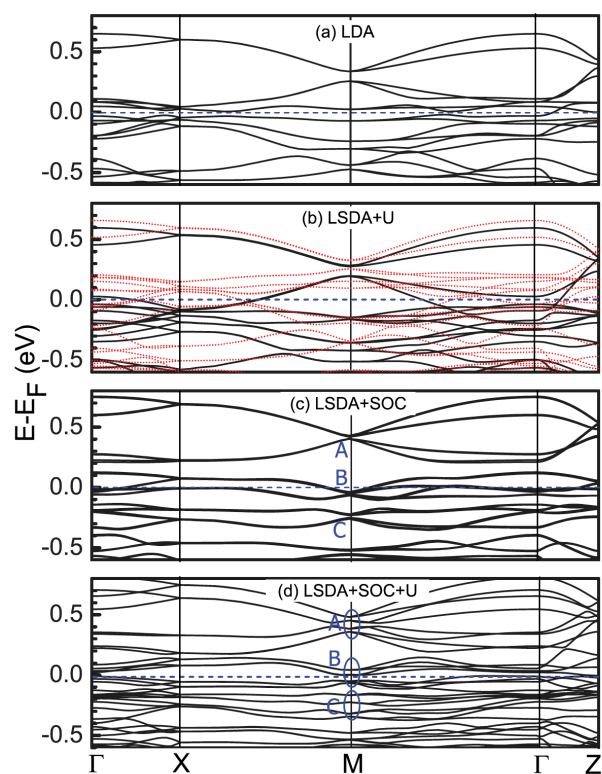
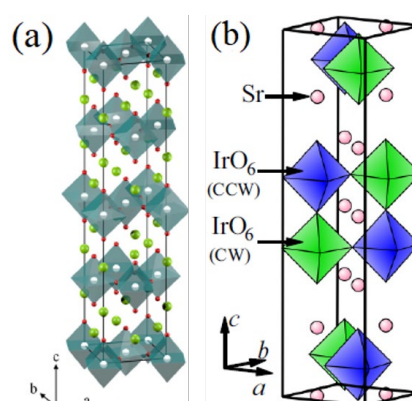


**Figure 8.** The calculated electronic band structures for  $\text{BaIrO}_3$  using (a) LDA, (b) LSDA + *U*, (c) LSDA + SOC, and (d) LSDA + SOC + *U*, where  $U = 2 \text{ eV}$ . The bands are plotted along  $\Gamma (0,0,0) - X (0.5,0,0) - M (0.5,0.5,0) - \Gamma (0,0,0) - Z (0,0,0.5)$ . The black solid and red dotted curves in (b) represent spin-up and spin-down channels, respectively. And the three letters (A, B, and C) in (c) and (d) show the three  $J_{\text{eff}} = 1/2$  bands. The binding energy in terms of  $E - E_F$ , so the occupied states have negative binding energies. Reprinted figure with permission from ref. 99. Copyright (2013) by the American Physical Society.

SOC + *U* (Figure 8d) for their first-principles calculations, with a value of *U* chosen to be  $2 \text{ eV}$ . Among these four possibilities, the one involving SOC and *U* (Figure 8d) was found to give the results that are consistent with the existing experimental observations on this system's electronic and magnetic behavior.<sup>43,89,90,96</sup> On a closer look, it can be discerned that a gap has opened up due to  $J_{\text{eff}} = 1/2$  spin-orbital Mott states, as is the case for  $\text{Sr}_2\text{IrO}_4$  (as discussed below) among other compounds,<sup>100</sup> for much of the Brillouin zone, leading to a picture consistent with the pseudo gap of Maiti *et al.*<sup>43</sup>

### $\text{Sr}_{n+1}\text{Ir}_n\text{O}_{3n+1}$ ( $n = 1, 2, \infty$ )

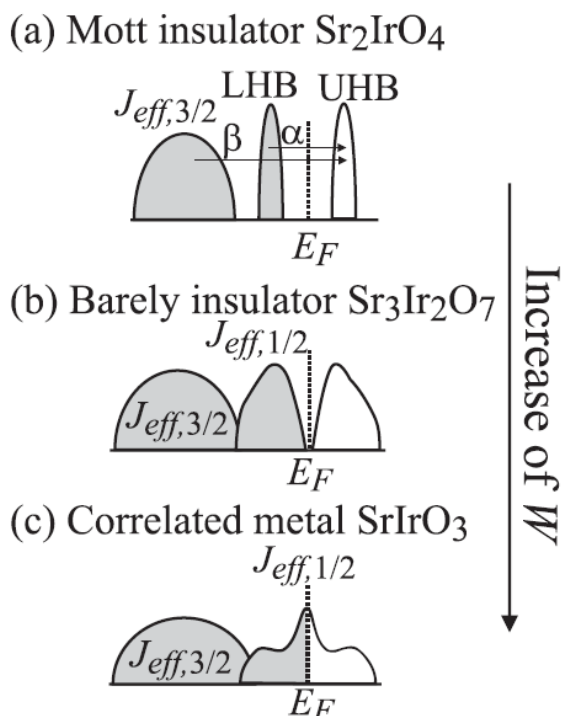
The Ruddlesden–Popper perovskite series of iridates  $\text{Sr}_{n+1}\text{Ir}_n\text{O}_{3n+1}$  show different properties depending on the value of *n*. Moon *et al.*<sup>36</sup> used optical spectroscopy and first-principles calculations to study the electronic structure of some of the 5*d* Ruddlesden–Popper series, and this study predicts existence of dimensionality-controlled MIT in these systems. In another such investigation, Kim *et al.*<sup>35</sup> used ARPES, optical conductivity, x-ray absorption measurements, and first-principles band structure calculations to study the electronic structure of  $\text{Sr}_2\text{IrO}_4$  ( $n = 1$ ). In fact, the band structure of  $\text{Sr}_2\text{IrO}_4$  ( $n = 1$ ) is among the more heavily investigated iridates.<sup>1–3,101–104</sup> Building up on these studies, Kim *et al.*<sup>37</sup> conducted studies of the phase factor, associated with a quantum state of  $\text{Sr}_2\text{IrO}_4$ . In an effort to provide deeper insights, Wang *et al.*<sup>5</sup> studied  $\text{Sr}_2\text{IrO}_4$  ( $n = 1$ ) (crystal structure shown in Figure 9a)<sup>105</sup> and  $\text{Sr}_3\text{Ir}_2\text{O}_7$  ( $n = 2$ ) (crystal structure shown in Figure 9b),<sup>106</sup> using ARPES, to determine the intracell and intercell coupling parameters along with electron correlation and gap sizes. In another study<sup>106</sup> that focused on deciphering the surface states of  $\text{Sr}_3\text{Ir}_2\text{O}_7$ , it was concluded that the near-surface of  $\text{Sr}_3\text{Ir}_2\text{O}_7$  is weakly metallic as opposed to the case for the  $\text{Sr}_2\text{IrO}_4$  surface state, which shows insulating behaviour of the Mott kind.<sup>107,108</sup> Furthermore, the collective magnetic excitations in  $\text{Sr}_2\text{IrO}_4$ <sup>109,110</sup> and  $\text{Sr}_3\text{Ir}_2\text{O}_7$ <sup>111</sup> have been probed using the resonant inelastic x-ray scattering. Yet, in terms of band structure,  $\text{SrIrO}_3$  ( $n = \infty$ ) is certainly the Ruddlesden–Popper perovskite given considerable attention.



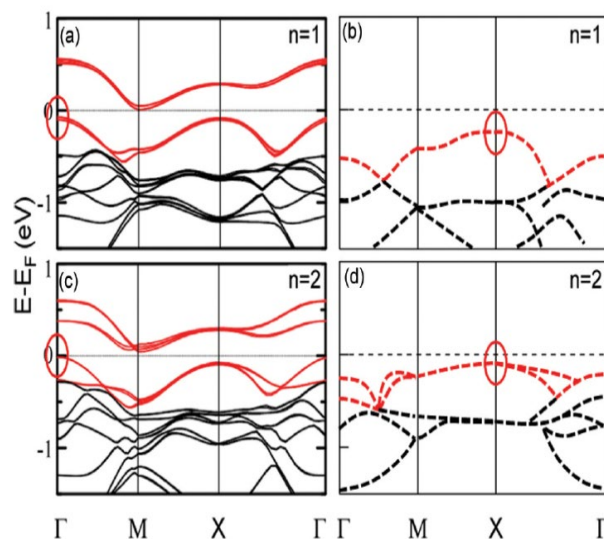
**Figure 9.** (a) Crystal structure of  $\text{Sr}_2\text{IrO}_4$ , where the  $\text{IrO}_6$  layers (grey = Ir; red = O) are separated by Sr atoms (light green). The  $\text{IrO}_6$  octahedra are rotated by  $12^\circ$  about the *c* axis.<sup>105</sup> © IOP Publishing. Reproduced with permission. All rights reserved. (b) Crystal structure of  $\text{Sr}_3\text{Ir}_2\text{O}_7$ , where CCW (CW) denote counterclockwise (clockwise) rotation of the  $\text{IrO}_6$  by  $12^\circ$ . Reprinted figure with permission from ref. 106. Copyright (2014) by the American Physical Society.

$\text{SrIrO}_3$ , which exhibits strong SOC limit, has been found to exist in a novel semimetallic phase based on the transport measurements carried out by Jian Liu *et al.*<sup>112</sup> Inspired by this study, Nie *et al.*<sup>15</sup> used *in situ* ARPES to investigate the electronic structure of metastable perovskite iridate  $\text{SrIrO}_3$ , as did Z.T. Liu *et al.*<sup>14</sup> These studies of  $\text{SrIrO}_3(100)$  films provide insight into effective hole mass and Fermi level placement that provide a context for the transport measurements on the monoclinic  $\text{SrIrO}_3$  reported by Takayama *et al.*<sup>16</sup> Recent investigation of high-quality epitaxial orthorhombic  $\text{SrIrO}_3(001)$  thin film strained on  $\text{SrTiO}_3$ , carried out by Evans *et al.*,<sup>113</sup> its surface termination, electronic structure, and crystal symmetry were examined using HR-ARPES, angle-resolved x-ray photoemission spectroscopy, and low energy electron diffraction (LEED), suggesting the surface electronic structure differs from the  $\text{SrIrO}_3(001)$  interface. This study<sup>113</sup> adds to the thickness-dependent studies conducted of the electronic structure independently by Schütz *et al.*,<sup>88</sup> Groenendijk *et al.*,<sup>114</sup> and Zhang *et al.*<sup>115</sup>

Since  $5d$  orbitals are spatially more extended than  $3d$  and  $4d$  orbitals, and thus more itinerant, the electron correlation is (at first glance) supposed to play a smaller role in description of these systems. Therefore, one can say,  $5d$  TMOs will have metallic ground states that can be easily understood by following the existing simple band theory. However,  $\text{Sr}_2\text{IrO}_4$  and  $\text{Sr}_3\text{Ir}_2\text{O}_7$  are found to have insulating ground states,<sup>44,101,116</sup>



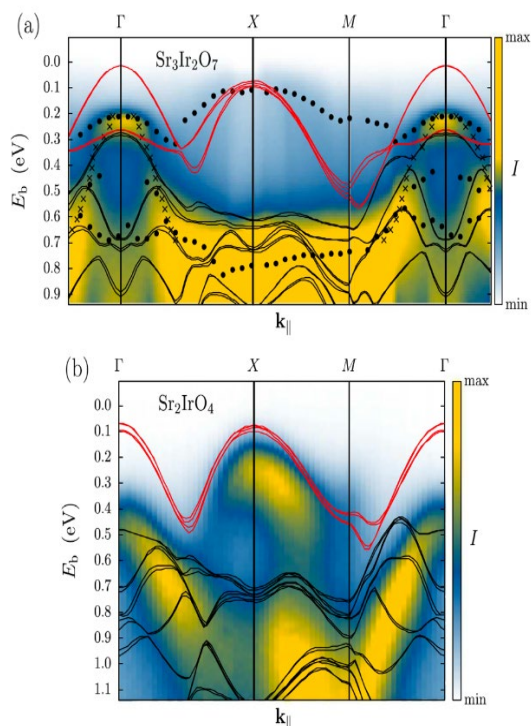
**Figure 10.** The schematic band diagrams for the  $\text{Sr}_{n+1}\text{Ir}_n\text{O}_{3n+1}$  compounds, which are described using effective total angular momentum number  $J_{\text{eff}}$  and strong SOC: (a) depicts that  $\text{Sr}_2\text{IrO}_4$  is a Mott insulator whereas, (b)  $\text{Sr}_3\text{Ir}_2\text{O}_7$  is barely an insulator, and (c)  $\text{SrIrO}_3$  is a correlated metal. Here,  $E_F$  shows the Fermi level and the direction of bandwidth ( $W$ ) increase (or interaction ( $U$ ) decrease) is indicated by the arrow. Reproduced from Ref. 36. Copyright (2008) by the American Physical Society.



**Figure 11.** (a), (c) The LDA +  $U$  + SOC band structure calculations for  $\text{Sr}_2\text{IrO}_4$  ( $n = 1$ ) and  $\text{Sr}_3\text{Ir}_2\text{O}_7$  ( $n = 2$ ), adopted from<sup>36</sup> (b), (d) The experimental dispersion data (centroids of spectral weight) for  $\text{Sr}_2\text{IrO}_4$  ( $n = 1$ ) and  $\text{Sr}_3\text{Ir}_2\text{O}_7$  ( $n = 2$ ). Here, the red lines represent the  $J_{\text{eff}} = 1/2$  bands whereas the black lines represent  $J_{\text{eff}} = 3/2$  bands. Calculations depict that the dominant states near the top of the valence band are at the  $\Gamma$  point (red ovals in (a) and (c)), while the experiments depict that the dominant low energy states are at the X point (red ovals in (b) and (d)) instead. Reprinted figure with permission from ref. 5. Copyright (2013) by the American Physical Society.

whereas  $\text{SrIrO}_3$  is shown to possess semimetallic ground state.<sup>14,15,112,117,118</sup> In Figure 10, the effective total angular momentum number ( $J_{\text{eff}}$ ) has been used to describe states arising in  $\text{Sr}_{n+1}\text{Ir}_n\text{O}_{3n+1}$  systems due to the presence of strong SOC. Figure 10a shows the splitting of the narrow  $J_{\text{eff}}$  bands into a lower Hubbard band (LHB) and an upper Hubbard band (UHB) as an effect of the  $U$  term, which, in turn, opens up the Mott gap<sup>107,108</sup> rendering  $\text{Sr}_2\text{IrO}_4$  ( $n = 1$ ) to be a Mott insulator. In Figure 10b, the increase in bandwidth ( $W$ ) and a decrease in the value of  $U$  term for the  $\text{Sr}_3\text{Ir}_2\text{O}_7$  ( $n = 2$ ) system, in comparison with the  $\text{Sr}_2\text{IrO}_4$  system, leaves the  $\text{Sr}_3\text{Ir}_2\text{O}_7$  system barely insulating. Figure 10c describes  $\text{SrIrO}_3$  ( $n = \infty$ ) as a correlated metal, since in this system the increase in  $W$  is predicted to outweigh the  $U$  term.

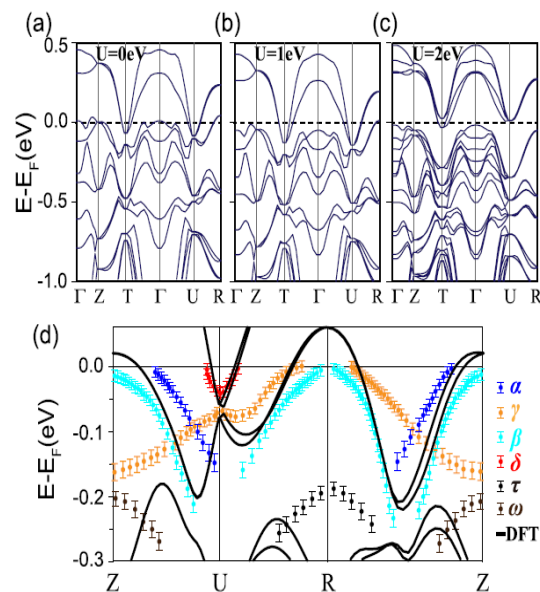
Theoretical band structure calculations for the  $\text{Sr}_2\text{IrO}_4$  and  $\text{Sr}_3\text{Ir}_2\text{O}_7$  systems (where  $U = 2.0$  eV and the SOC constant was suggested to have a value of 0.4 eV) are shown in Figure 11a and Figure 11c,<sup>5,36</sup> while the experimentally extracted in-plane band dispersion data are shown in Figure 11b and Figure 11d.<sup>5</sup> In these calculations,<sup>1-3,36</sup> the strong SOC splits the Ir  $5d$   $t_{2g}$  band into what are effectively  $J_{\text{eff}} = 1/2$  and  $J_{\text{eff}} = 3/2$  bands. As noted at the outset, the half-filled  $J_{\text{eff}} = 1/2$  band, near the Fermi level  $E_F$ , is found to split into what amounts to lower and upper Hubbard bands, because of its extremely small effective bandwidth even though the on-site Coulombic repulsion is relatively small.<sup>1-3,5</sup> Interestingly, the calculated band structure matches the experimentally derived band dispersion data for both the iridate systems without any discernible shifting of the bands or rescaling. It can be inferred from Figure 11 that there is no band crossing at the Fermi level, which indicates (and is consistent with) the insulating behaviour of these iridate systems. Furthermore, the ARPES data (see Figure 12), from an



**Figure 12.** The experimental ARPES spectra for (a)  $\text{Sr}_3\text{Ir}_2\text{O}_7$  ( $h\nu = 10.5$  eV,  $T = 9$  K) and (b)  $\text{Sr}_2\text{IrO}_4$  ( $h\nu = 85$  eV,  $T = 100$  K). Here, solid lines represent the calculated band structures<sup>34</sup>: bands with  $J_{\text{eff}} = 1/2$  are in red and those with  $J_{\text{eff}} = 3/2$  in black. Also, the bullets (in (a)) represent the local curvature maxima of the concave parts of the energy distribution curves (EDCs) and the crosses represent the momentum distribution curve (MDC) peaks for the binding energies ranging between 0.2 eV–0.7 eV near the  $\Gamma$  point.<sup>104</sup> Binding energies are in terms of  $E_F - E$ ; thus, the occupied states have positive binding energies, and in this regard differ from the other experimental band structure representations.<sup>115</sup> © IOP Publishing. Reproduced with permission. All rights reserved.

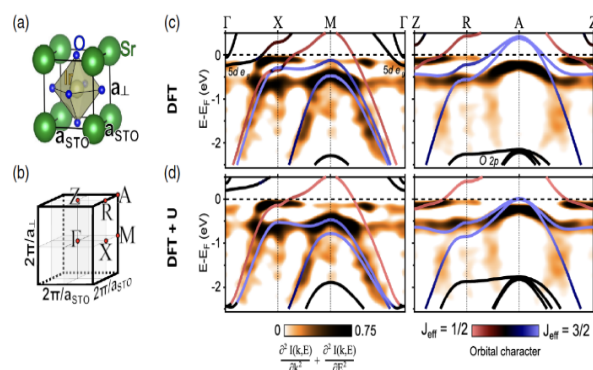
independent study carried out by Wojek *et al.*,<sup>119</sup> found that the in-plane electronic structure of  $\text{Sr}_3\text{Ir}_2\text{O}_7$  was consistent with theory.<sup>36</sup>

Figure 13 compares the density functional theory band structure, for orthorhombic perovskite  $\text{SrIrO}_3$  films, with the results of ARPES measurements taken on  $\text{SrIrO}_3(100)$  films grown strontium titanate (STO) by means of oxide molecular beam epitaxy.<sup>14</sup> Figure 14 depicts the experimental and theoretical band structures obtained via soft-x-ray angle-resolved photoelectron spectroscopy (i.e. using photon energies greater than is typical for ARPES) on a 9-unit-cell-thick  $\text{SrIrO}_3$  film.<sup>88</sup> Figure 15 shows the experimental valence band electronic structure of a 5 nm thick orthorhombic  $\text{SrIrO}_3(001)$  film that was derived from another set of ARPES measurement.<sup>113</sup> Figure 16 shows the angle-resolved photoemission of  $\text{SrIrO}_3(001)$  thin films also grown on  $\text{SrTiO}_3(001)$ . The band structure of even  $\text{SrIrO}_3(001)$  thin films is seen to have wave vector dependence both in-plane (i.e.,  $k_x$ , as in Figure 16c), and also dependent on wave vector along the surface normal (i.e.,  $k_z$ , as in Figure 16a). This evidence for band structure is seen in the binding energy shifts of the occupied states that are dependent on photon energy, as seen in Figure 16a. This is representative of the  $\text{SrIrO}_3(001)$  thin film retaining bulk band structure character. This is especially apparent for the state near the top of the valence band. These state near the top



**Figure 13.** DFT band structure calculations and the experimental results for the valence band. (a)–(c) Represent DFT band structure calculations of orthorhombic perovskite  $\text{SrIrO}_3$  films for (a)  $U = 0$  eV, (b)  $U = 1$  eV, and (c)  $U = 2$  eV. (d) The comparison of results of ARPES measurements with the DFT calculations (for  $U = 0$  eV) along the high-symmetry directions in epitaxial  $\text{SrIrO}_3$  films. Here, solid lines represent DFT calculations. Reproduced from ref. 14. CC BY 4.0

of the valence band disperse with wave vector along the surface normal (i.e.,  $k_z$ ), i.e., have a wave vector dependence that varies with photon energy indicative of a bulk character, as plotted in Figure 16b. The dispersion of the states, with changing wave vector in-plane (Figure 16c), match those bands seen near the top of the valence band as a function of polar angle as in Figure 14, and Figure 15. This is quite distinct from what was observed for  $\text{Ba}_2\text{IrO}_4$ .<sup>88</sup> There is general agreement that  $\text{SrIrO}_3(100)$  is surface terminated and superperiodicities can appear in the thinner films grown on  $\text{SrTiO}_3(100)$ , and the experimental band structures of these various experimental band structure



**Figure 14.** (a) Real and (b) reciprocal space structure of strained, tetragonal  $\text{SrIrO}_3$  in absence of octahedral rotations. (c) Experimental  $E$  vs  $k$  dispersions along the high-symmetry lines  $\Gamma - X - M - \Gamma$  and  $Z - R - A - Z$  obtained using soft X-ray ARPES ( $h\nu = 745$  eV) compared with calculated band structure (using DFT +  $U$ ) for the tetragonal setting with  $U = J = 0$  eV. (d) The X-ray ARPES derived band structure ( $h\nu = 660$  eV) is compared with the calculated band structure with  $U = 3.4$  eV and  $J = 0.4$  eV. Introducing sizeable on-site Coulomb repulsion enhances the agreement between the theoretical and experimental results. Reprinted figure with permission from ref. 88. Copyright (2017) by the American Physical Society.

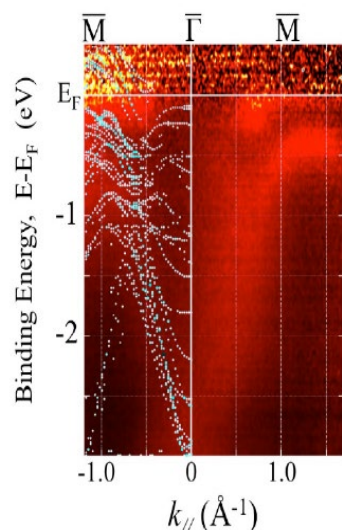


**Figure 15.** The experimental valence band electronic structure of a 5 nm thick orthorhombic SrIrO<sub>3</sub>(001) film, derived from ARPES. Results of the DFT band structure calculations are superimposed on the experimental data (on the left), where the intensity of the blue circles represents greater contributions to the spectral weight. Reproduced from ref. 113. CC BY 4.0

measurements are similar as is evident from a comparison of Figures 14, 15, and 16.

While the surface band structure of SrIrO<sub>3</sub>(001) has been noted to resemble Ba<sub>2</sub>IrO<sub>4</sub>,<sup>88</sup> as noted above, no bulk band structure was observed Ba<sub>2</sub>IrO<sub>4</sub>,<sup>7</sup> while for SrIrO<sub>3</sub>(001), there is evidence for a bulk band structure even in 5 nm thick films (Figure 16). Having established that there exists an evolving lattice distortion in high quality epitaxial orthorhombic SrIrO<sub>3</sub>(001) thin films fully strained on SrTiO<sub>3</sub>(001),<sup>86,95</sup> so the oxygen octahedra (IrO<sub>6</sub>) tilt significantly across the 12 monolayers film, then an absence of a bulk band structure should be possible as then there is no conserved wave vector. As indicated in Figures 14 and 15, the surface Brillouin zone, evident from the experimental band structure, is consistent with the (001) surface, as but not with the superperiodicity determined LEED.<sup>88,113</sup> So the band structure seems insensitive to perturbations caused by IrO<sub>6</sub> oxygen octahedra that tilt,<sup>113</sup> i.e., the reconstructions evident in the extra diffraction spots in the LEED reported elsewhere.<sup>88,113</sup> In spite of the oxygen octahedra tilt, as indicated by the extra diffraction spots in the LEED,<sup>88,113</sup> there is strong evidence for a bulk band structure in 5 nm thick SrIrO<sub>3</sub>(001) thin films grown on SrTiO<sub>3</sub>(001), as just noted.

Generally, Sr<sub>2</sub>IrO<sub>4</sub> and Sr<sub>3</sub>Ir<sub>2</sub>O<sub>7</sub> are found to have insulating ground states. However, based on both theoretical and experimental band structure studies by Jian Liu *et al.*,<sup>112</sup> Nie *et al.*,<sup>15</sup> and Z.T. Liu *et al.*,<sup>14</sup> it can be concluded that the perovskite structured SrIrO<sub>3</sub> has a semimetallic ground state. This tends to differ somewhat from the claims made by Moon *et al.*,<sup>36</sup> based on the result of their theoretical calculations, that the perovskite structured SrIrO<sub>3</sub> system has a correlated metallic ground state. The disparity between theory<sup>36</sup> and experiment<sup>112</sup> implies that the strong SOC is, indeed, responsible for the dimensionality-controlled (film thickness dependent) MIT, but interface strain and surface to volume effects cannot be excluded.<sup>113,115</sup> The effect of dimensionality on electronic properties

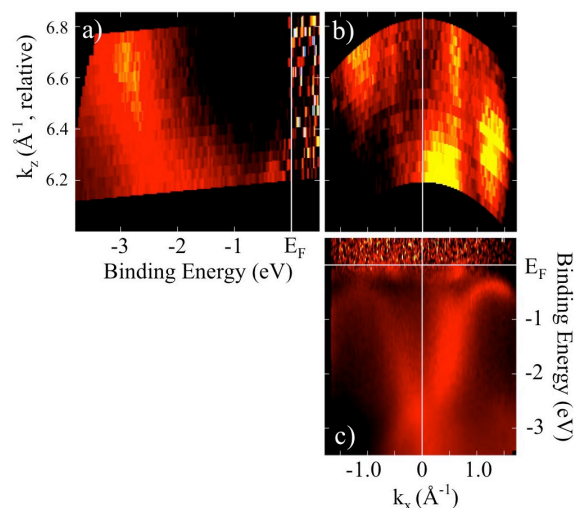


**Figure 16.** Evidence for a bulk band structure in thin films of SrIrO<sub>3</sub>(001). (a) the photon energy dependence providing a  $k_z$  mapping for the states near the centre of the Brillouin zone, (b) the wave vector  $k_x$ - $k_y$  mapping for the states near the top of the valence band, and (c) the expected  $k_x$  band structure mapping. The measurements were performed at room temperature.

of these iridates is further revealed in a study by Matsuno *et al.*,<sup>120</sup> where a semimetal-magnetic insulator transition is observed as the dimensions of the SrIrO<sub>3</sub> are varied. It has been widely observed that the SrIrO<sub>3</sub>(001) film epitaxially grown on the STO substrate is Sr-O surface terminated,<sup>113</sup> and this results in a huge surface to bulk core level shift of  $\sim 1.5$  eV.<sup>113</sup> It may well be that this surface termination may be responsible, at least in part, for the thickness-driven MIT discussed elsewhere.<sup>88,114</sup> We note, in passing, that studies conducted by Kim *et al.*,<sup>121</sup> Liu *et al.*,<sup>122</sup> Cao *et al.*,<sup>123</sup> Terashima *et al.*,<sup>102</sup> and Martins *et al.*<sup>124</sup> suggest that Sr<sub>2</sub>IrO<sub>4</sub> may provide a valuable comparison with the cuprates.

### Alkali metal iridates: T<sub>2</sub>IrO<sub>3</sub> (T = Li, Na)

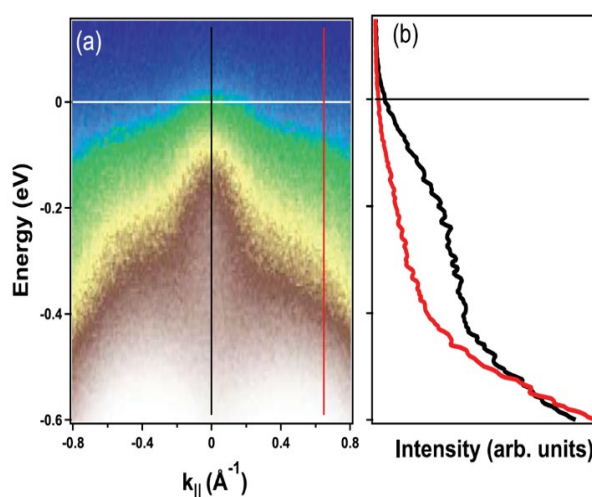


**Figure 17.** (a) Measured electronic band structure along the high symmetry  $\Gamma$ -M direction at a constant photon energy of 90 eV. (b) Energy distribution curves integrated over  $0.04 \text{ \AA}^{-1}$  around  $\Gamma$  (in black) and at  $0.65 \text{ \AA}^{-1}$  (in red). The binding energies are in terms of  $E - E_F$ ; thus, the occupied states have negative binding energies. Reprinted figure with permission from ref. 134. Copyright (2020) by the American Physical Society.

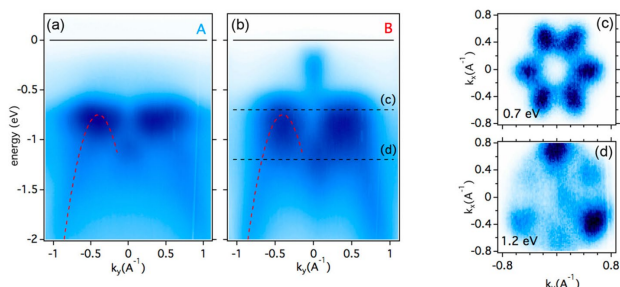


**Figure 18.** The angle-resolved photoemission valence band dispersion along  $k_y$  for the  $\text{Na}_2\text{IrO}_3$  iridate for the oxygen (a) and sodium (b) terminations. (c), (d) Constant energy maps in the vicinity of  $\Gamma$  at the two energies indicated by the dashed lines in (b). Reprinted figure with permission from ref. 137. Copyright (2017) by the American Physical Society.

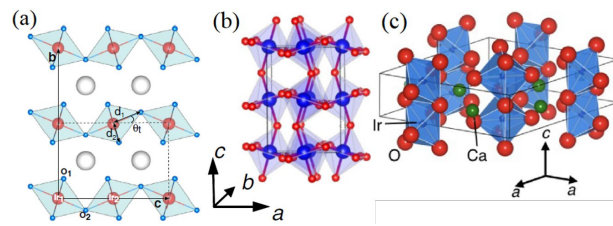


**Figure 19.** (a) Crystal structure of post-perovskite  $\text{CaIrO}_3$  projected on the  $bc$  plane where the primitive unit cell is indicated by dashed lines. Here, the large, medium, and small circles represent Ca, Ir, and O, respectively. Reprinted figure with permission from ref. 148. Copyright (2015) by the American Physical Society. (b) Crystal structure of perovskite  $\text{CaIrO}_3$ . Reproduced from ref. 141. CC BY 4.0. (c) Hexagonal crystal structure of  $\text{Ca}_2\text{IrO}_3$ .<sup>149</sup> © [2018] The Physical Society of Japan (J. Phys. Soc. Jpn. 87, 013703)

The alkali metal iridates, of the form  $\text{T}_2\text{IrO}_3$  ( $\text{T} = \text{Li}, \text{Na}$ ), are different from the iridates discussed above as the alkali metal iridates are the family of iridates with structures, including the honeycomb lattice,<sup>18,125</sup> not characteristic of perovskite structures adopted by many iridates. Among these iridates,  $\text{Li}_2\text{IrO}_3$  is found to have spiral ordering<sup>126</sup> while its sodium counterpart ( $\text{Na}_2\text{IrO}_3$ ) possesses a zigzag magnetic pattern.<sup>127</sup> Initial theoretical studies by Shitade *et al.*<sup>18</sup> suggested that these systems are quantum spin Hall insulators with topologically nontrivial electronic states, but are now thought to be magnetically ordered Mott insulators instead, based on experiment, with the antiferromagnetic ordering temperature,  $T_N$ , being 15 K.<sup>126,128</sup> Besides, a detailed study by Sohn and coworkers<sup>129</sup> proposed that the possibility of mixing of  $J_{\text{eff}} = 1/2$  and  $J_{\text{eff}} = 3/2$  states in explaining the ground state of  $\text{Na}_2\text{IrO}_3$  should not be discarded. In an experimental study carried out by Alidoust *et al.*,<sup>130</sup> the electronic band structure of  $\text{Na}_2\text{IrO}_3$  was shown to have six-fold symmetry owing to its honeycomb lattice. In spite of the transport measurements on  $\text{Na}_2\text{IrO}_3$ , indicating insulating behavior, the Fermi level crossing at  $\bar{\Gamma}$  by the surface electronic bands implies the

presence of metallic character at least at the boundary of  $\text{Na}_2\text{IrO}_3$ . These radically different claims about the electronic behavior of  $\text{Na}_2\text{IrO}_3$  can be simultaneously correct, because the transport measurements, unlike the photon energy dependent ARPES, provide insights into a system's behavior in the bulk as opposed to the characteristics of surface electronic states. It is totally possible to have a surface that is metallic when the bulk is not.<sup>131</sup> Moreover, a theoretical study by Li *et al.*<sup>132</sup> to analyze the optical conductivity for  $\text{Na}_2\text{IrO}_3$  and  $\text{Li}_2\text{IrO}_3$  suggests that, although the experimental data on electronic structure of  $\text{A}_2\text{IrO}_3$  materials look alike,<sup>133</sup> there are differences in their optical conductivity.<sup>132</sup>

Interestingly enough, a recent experimental study by Rodriguez *et al.*<sup>134</sup> which focused on finding the transport mechanism for  $\text{Na}_2\text{IrO}_3$  at temperatures above the antiferromagnetic ordering temperature ( $T_N \approx 15$  K), concluded that the main transport mechanism is in agreement with Mott's variable range hopping law. The ARPES data collected in the high temperature limit of around 290 K as the data indicates a very limited but nonetheless non-zero density of states at the Fermi level, as seen in Figure 17a, consistent with Mott variable range hopping.<sup>134</sup> Figure 17b shows energy

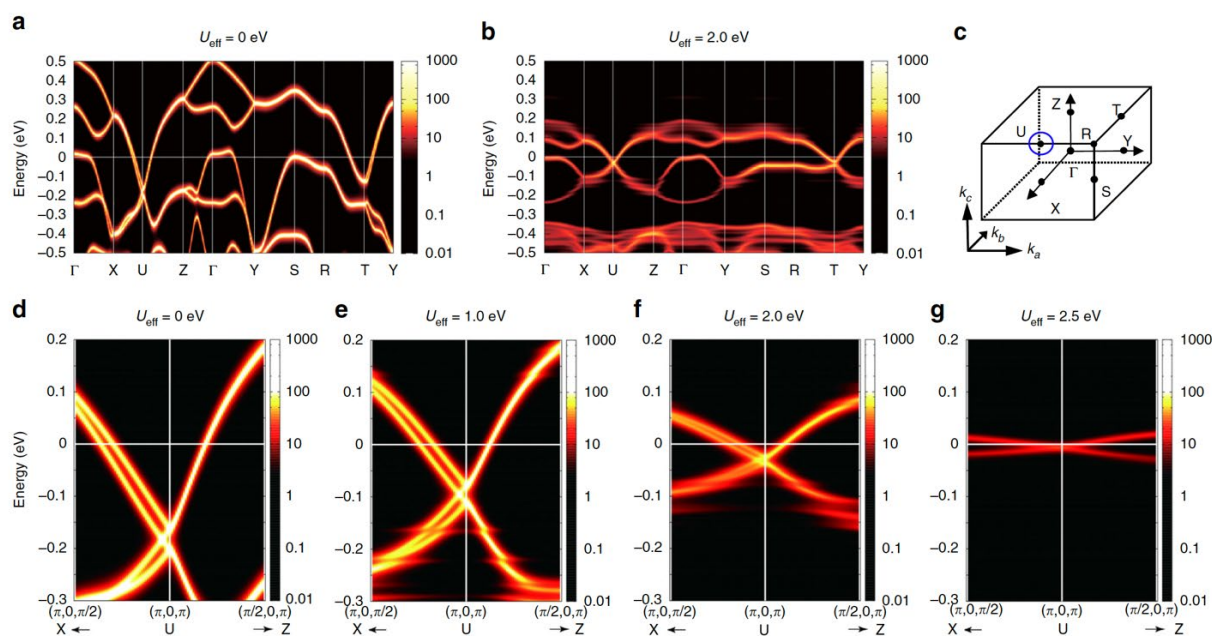


**Figure 20.** Band structure calculations based on density functional theory and dynamical mean field theory. (a, b) Overview of band structure calculations with  $U_{\text{eff}} = 0$  eV and 2 eV, where the scale bar depicts the magnitude of spectral function. (c) Momentum space illustration along with the Dirac line node (blue loop encircling the U-point). (d–g) Magnified view of band structure around the Dirac line node with different  $U_{\text{eff}}$ . The Dirac-like dispersion is significantly renormalized for  $U_{\text{eff}} = 2.5$  eV, which is a precursor phenomenon of the Mott criticality, and the averaged Fermi velocity values are  $2.0 \times 10^5$ ,  $1.8 \times 10^5$ ,  $8.1 \times 10^4$ , and  $2.0 \times 10^4$  m/s at  $U_{\text{eff}} = 0, 1.0, 2.0,$  and  $2.5$  eV, respectively. Reproduced from ref. 141. CC BY 4.0

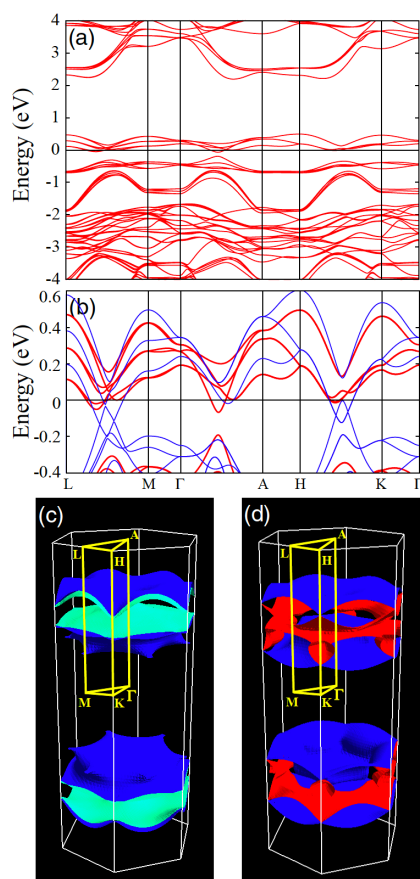


**Figure 21.** (a) Ab initio density functional band structure calculations incorporating the SOC effect for  $\text{Ca}_5\text{Ir}_3\text{O}_{12}$ . Here,  $E_F$  corresponds to the zero energy. (b) Zoomed-in view of the low-energy band structure, where the SO-GGA band (thick red curves) is compared with the GGA band (thin blue curves). (c) The calculated Fermi surface for SO-GGA, and (d) GGA. The SOC can resolve the band degeneracy, thus dark-blue and bright-blue colors in (c) are used to represent the bands with the same band character, whereas the GGA Fermi surface consists of two different bands (the dark-blue and dark-red colors in (d)). Also, the upper and lower objects in (c) and (d) represent the front and back sides at the surface, respectively.<sup>149</sup> © [2018] The Physical Society of Japan (J. Phys. Soc. Jpn. 87, 013703)

distribution curves (EDCs) indicating the existence of non-zero density of states at the Fermi level at  $\Gamma$  (black), as well as at a larger momentum value (red). The full picture of electronic properties of  $\text{Na}_2\text{IrO}_3$  is far from completely certain, as there are some existing discrepancies in reported band gaps<sup>135,136</sup> owing to the ease with which the alkali metal compounds may deteriorate. Furthermore, the ARPES results presented in this study<sup>134</sup> are consistent with higher resolution spatially resolved ARPES data shown in the investigation by Moreschini *et al.*<sup>137</sup> (Figure 18) which provides clear evidence of the metallic surface state.<sup>130</sup> This surface state for the  $\text{Na}_2\text{IrO}_3$  iridate insulator is termination dependent,<sup>137</sup> although other explanations have been implied,<sup>133</sup> yet note that Figure 17a does resemble Figure 18b.

Though  $\text{Li}_2\text{IrO}_3$  and  $\text{Na}_2\text{IrO}_3$  fall in the category of alkali metal iridates with honeycomb lattice and have similar electronic band structure,<sup>133</sup> they still exhibit discernable differences in their optical properties.<sup>132</sup> Moreover, spatially-resolved ARPES on  $\text{Na}_2\text{IrO}_3$  suggests the presence of quasiparticle formation in the system,<sup>134,137</sup> while EDCs indicate toward Mott's variable range hopping being the dominant transport mechanism for temperatures above the antiferromagnetic ordering temperature (15 K).<sup>134</sup>

## Iridates of calcium: $\text{CaIrO}_3$ and $\text{Ca}_5\text{Ir}_3\text{O}_{12}$

Among the various calcium iridates ( $\text{CaIrO}_3$ ,  $\text{Ca}_4\text{IrO}_6$ , and  $\text{Ca}_5\text{Ir}_3\text{O}_{12}$ ), the band structure investigations have been emphasized on  $\text{CaIrO}_3$  and  $\text{Ca}_5\text{Ir}_3\text{O}_{12}$ . Both  $\text{CaIrO}_3$  and  $\text{Ca}_5\text{Ir}_3\text{O}_{12}$  exist in different crystal structures, i.e.  $\text{CaIrO}_3$  is found to stabilize in post-perovskite ( $Cmcm$ )<sup>138–140</sup> (Figure 19a) and perovskite ( $Pbnm$ )<sup>139,141–143</sup> (Figure 19b) crystal structures, whereas  $\text{Ca}_5\text{Ir}_3\text{O}_{12}$  has an hexagonal ( $P\bar{6}2m$ )<sup>144–146</sup> crystal structure (Figure 19c).

Initial theoretical investigations conducted independently by A. Subedi,<sup>140</sup> Sala *et al.*,<sup>147</sup> and Kim *et al.*<sup>148</sup> suggested that the post-perovskite  $\text{CaIrO}_3$  possesses an insulating ground state, whereas recent experiments by Fujioka *et al.*<sup>141</sup> have shown that perovskite  $\text{CaIrO}_3$  (with  $\text{GdFeO}_3$ -type lattice distortion) exists as a Dirac semimetal. The latter study<sup>141</sup> implied the presence of strong electron correlation, in addition to SOC, and indicated that very high electron mobilities, as high as  $60,000 \text{ cm}^2\text{V}^{-1}\text{s}^{-1}$ , are possible for  $\text{CaIrO}_3$ . Regrettably, this high mobility, for  $\text{CaIrO}_3$ , is so far indicated only well below 100 K. This result is somewhat counterintuitive, for one would expect a decrease in electron mobility of a system as a consequence of strong electron correlation. The results of band structure calculations conducted by Fujioka *et al.*<sup>141</sup> using density functional theory along with dynamical mean field theory are shown in Figure 20. Band structure calculations with  $U_{\text{eff}} = 0 \text{ eV}$  and  $U_{\text{eff}} = 2 \text{ eV}$  are shown in Figures 20a and 20b, respectively, while Figure 18c depicts the Dirac line node (blue loop encircling the U-point). Magnified view of the band structure along the Dirac line node (near the U-point) with different values of  $U_{\text{eff}}$  is also shown (Figures 18d–g). Thus, it can be seen that the Dirac-like dispersion is renormalized as the Dirac line node approaches the Fermi energy, but the increase in  $U_{\text{eff}}$  is accompanied by a decreasing Fermi velocity.<sup>141</sup> The averaged Fermi velocity ( $v_F$ ) is found to drop by an order of magnitude (from  $2.0 \times 10^5 \text{ m/s}$  to  $2.0 \times 10^5 \text{ m/s}$ ) as the value of  $U_{\text{eff}}$  changes from 0 eV to 2.5 eV.

$\text{Ca}_5\text{Ir}_3\text{O}_{12}$  is a semiconductor with two-phase transitions,<sup>144</sup> one of which is an antiferromagnet with  $T_N = 7.8 \text{ K}$ ,<sup>144–146</sup> while the other is a second-order phase transition at 105 K related to sharp anomaly in specific heat along with a change electrical resistivity.<sup>144,145,149</sup> The origins for such anomalous behaviour, associated with the temperature phase transition, are not completely identified.<sup>150</sup> Moreover, recently, Matsuhira *et al.*<sup>149</sup> calculated the electronic band structure for  $\text{Ca}_5\text{Ir}_3\text{O}_{12}$  (Figure 21) as well as discovered the existence of nonlinear conductivity along the  $c$ -axis of this system. The electronic band structure obtained after implementation of the SOC effect to density functional theory calculations is shown in Figure 21a, while the comparison between the SO-GGA band (thick red curves) and the GGA band (thin blue curves) is shown in Figure 21b, and their respective Fermi surfaces are shown in Figures 21c and 21d.

On the whole, exceedingly high electron mobility of  $60,000 \text{ cm}^2\text{V}^{-1}\text{s}^{-1}$  for  $\text{CaIrO}_3$  (which is the largest among the oxide semiconductors),<sup>141</sup> due to the presence of strong electron correlation and SOC, is pivotal as provides further motivation for research on exotic quantum phenomena in topological materials. And as far as  $\text{Ca}_5\text{Ir}_3\text{O}_{12}$  is concerned, despite the great efforts reported in investigations by Hanate *et al.*<sup>150</sup> and Hasegawa *et al.*<sup>151</sup> there is still work to be done in order to decipher the mystery behind its anomalous behavior at 105 K. A better understanding of  $\text{Ca}_5\text{Ir}_3\text{O}_{12}$  is important since it is the only pseudo-one-dimensional iridate known so far, which represents a rather unique situation accompanied by potentially interesting electronic and magnetic properties.<sup>144</sup>

## Conclusions

The interplay between electron correlation, SOC, crystal field splitting, octahedral distortion, and bandwidth, along with a possibility of inter-site hopping in 5d TMOs have made the investigation of the band structure of many iridates quite compelling. As noted throughout this review, there is evidence of dimensionality related metal-nonmetal transitions.<sup>15,86,97</sup> Clearly perturbations to the band structure can alter the insulating or semimetallic behavior. As is evident, the theoretical band structure studies are not always successful in correctly predicting the electronic structure, as was seen in the studies of the pyrochlore iridates ( $A_2Ir_2O_7$ )<sup>19</sup> and  $SrIrO_3$ .<sup>36</sup> Strain, surface termination, octahedral distortions, and film thickness all can affect experiment, especially in thin films.

What is indicated for future work is more photon energy dependent experimental band structure measurements to explore the surface band structure as well as better identify the bulk band dispersion. It is so far very clear that the surface is different from the bulk for many iridates, even for very thin films. Surface states would not disperse with photon energy and then they might be distinguished from more bulk-like states. Furthermore, band structure calculations that are slab thickness dependent and identify surface states that do not fall into a gap of the projected bulk band structure would be of interest. If there is evidence of surface states or strong surface resonance, then the possibility of interface states must be recognized. Interface states could have a profound effect on potential device properties, especially if the iridate is either dielectric or semiconducting. A surface electronic structure leading to a distinct interface electronic structure also opens the door to a Schottky barrier formation that may also act as a spin filter.<sup>152</sup>

Moreover, there are some other iridates to explore,<sup>3</sup> like the double-perovskites (bearing the general formula: either  $A_2B_1rO_6$  or  $AA'B_1rO_6$ )<sup>153</sup> for which there are a few theoretical calculations,<sup>154–156</sup> but no experimental band structure. Also, a detailed study and analysis of electron mobilities of topological materials, like some of the iridates, should be something to focus on in the future because now we know that as opposed to one's expectations, strongly correlated systems can show surprisingly high mobility as was reported by Fujioka *et al.*<sup>141</sup> for  $CaIrO_3$ .

## Conflicts of interest

There are no conflicts of interest to declare.

## Acknowledgements

This work was supported by NSF through the Nebraska Materials Research Science and Engineering Center (MRSEC) Grant No. DMR-1420645 (structural, spectroscopy, and DFT studies), and NSF Grant No. DMR-1710461 (sample growth and characterization). The research was performed in part in the Nebraska Nanoscale Facility: National Nanotechnology Coordinated Infrastructure and the Nebraska Center for Materials and Nanoscience, which are supported by the National Science Foundation under Award ECCS: 1542182, and the Nebraska Research Initiative. The experiments have been performed under the approval of HiSOR (Proposal No. 18BG005 and 18BG006).

## References

- 1 B. Lenz, C. Martins and S. Biermann, *J. Phys. Condens. Matter*, 2019, **31**, 293001. DOI:10.1088/1361-648X/ab146a
- 2 C. Martins, M. Aichhorn, L. Vaugier and S. Biermann, *Phys. Rev. Lett.*, 2011, **107**, 266404. DOI:10.1103/PhysRevLett.107.266404
- 3 C. Martins, M. Aichhorn and S. Biermann, *J. Phys. Condens. Matter*, 2017, **29**, 263001. DOI:10.1088/1361-648X/aa648f
- 4 Q. Wang, Y. Cao, X. G. Wan, J. D. Denlinger, T. F. Qi, O. B. Korneta, G. Cao and D. S. Dessau, *J. Phys. Condens. Matter*, 2015, **27**, 015502. DOI:10.1088/0953-8984/27/1/015502
- 5 Q. Wang, Y. Cao, J. A. Waugh, S. R. Park, T. F. Qi, O. B. Korneta, G. Cao and D. S. Dessau, *Phys. Rev. B - Condens. Matter Mater. Phys.*, 2013, **87**, 1–6. DOI:10.1103/PhysRevB.87.245109
- 6 A. Georges, L. de' Medici and J. Mravlje, *Annu. Rev. Condens. Matter Phys.*, 2013, **4**, 137–178. DOI:10.1146/annurev-conmatphys-020911-125045
- 7 S. Moser, L. Moreschini, A. Ebrahimi, B. Dalla Piazza, M. Isobe, H. Okabe, J. Akimitsu, V. V. Mazurenko, K. S. Kim, A. Bostwick, E. Rotenberg, J. Chang, H. M. Rønnow and M. Groni, *New J. Phys.*, 2014, **16**, 013008. DOI:10.1088/1367-2630/16/1/013008
- 8 M. Imada, A. Fujimori and Y. Tokura, *Rev. Mod. Phys.*, 1998, **70**, 1039–1263. DOI:10.1103/RevModPhys.70.1039
- 9 I. Kézsmárki, N. Hanasaki, D. Hashimoto, S. Iguchi, Y. Taguchi, S. Miyasaka and Y. Tokura, *Phys. Rev. Lett.*, 2004, **93**, 266401. DOI: 10.1103/PhysRevLett.93.266401
- 10 A. Fujimori, I. Hase, H. Namatame, Y. Fujishima, Y. Tokura, H. Eisaki, S. Uchida, K. Takegahara and F. M. F. de Groot, *Phys. Rev. Lett.*, 1992, **69**, 1796–1799. DOI:10.1103/PhysRevLett.69.1796
- 11 J. S. Lee, Y. S. Lee, T. W. Noh, K. Char, J. Park, S.-J. Oh, J.-H. Park, C. B. Eom, T. Takeda and R. Kanno, *Phys. Rev. B*, 2001, **64**, 245107. DOI:10.1103/PhysRevB.64.245107
- 12 T. F. Qi, O. B. Korneta, X. Wan, L. E. DeLong, P. Schlottmann and G. Cao, *J. Phys. Condens. Matter*, 2012, **24**, 345601. DOI:10.1088/0953-8984/24/34/345601
- 13 J. M. Kahk, C. G. Poll, F. E. Oropeza, J. M. Ablett, D. Céolin, J. P. Rueff, S. Agrestini, Y. Utsumi, K. D. Tsuei, Y. F. Liao, F. Borgatti, G. Panaccione, A. Regoutz, R. G. Egdell, B. J. Morgan, D. O. Scanlon and D. J. Payne, *Phys. Rev. Lett.*, 2014, **112**, 117601. DOI:10.1103/PhysRevLett.112.117601
- 14 Z. T. Liu, M. Y. Li, Q. F. Li, J. S. Liu, W. Li, H. F. Yang, Q. Yao, C. C. Fan, X. G. Wan, Z. Wang and D. W. Shen, *Sci. Rep.*, 2016, **6**, 30309. DOI:10.1038/srep30309
- 15 Y. F. Nie, P. D. C. King, C. H. Kim, M. Uchida, H. I. Wei, B. D. Faeth, J. P. Ruf, J. P. C. Ruff, L. Xie, X. Pan, C. J. Fennie, D. G. Schlom and K. M. Shen, *Phys. Rev. Lett.*, 2015, **114**, 016401. DOI:10.1103/PhysRevLett.114.016401
- 16 T. Takayama, A. N. Yaresko and H. Takagi, *J. Phys. Condens. Matter*, 2019, **31**, 074001. DOI:10.1088/1361-648X/aaf68a
- 17 F. Wang and T. Senthil, *Phys. Rev. Lett.*, 2011, **106**, 136402. DOI:10.1103/PhysRevLett.106.136402
- 18 A. Shitade, H. Katsura, J. Kuneš, X.-L. Qi, S.-C. Zhang and N. Nagaosa, *Phys. Rev. Lett.*, 2009, **102**, 256403. DOI:10.1103/PhysRevLett.102.256403
- 19 B. J. Yang and Y. B. Kim, *Phys. Rev. B - Condens. Matter Mater. Phys.*, 2010, **82**, 085111. DOI:10.1103/PhysRevB.82.085111
- 20 Y. Ando, *J. Phys. Soc. Japan*, 2013, **82**, 102001. DOI:10.7566/JPSJ.82.102001
- 21 N. Kumar, S. N. Guin, K. Manna, C. Shekhar and C. Felser, *Chem. Rev.*, 2020. DOI:10.1021/acs.chemrev.0c00732
- 22 D. Pesin and L. Balents, *Nat. Phys.*, 2010, **6**, 376–381. DOI:10.1038/nphys1606
- 23 H.-C. Jiang, Z.-C. Gu, X.-L. Qi and S. Trebst, *Phys. Rev. B*, 2011, **83**, 245104. DOI:10.1103/PhysRevB.83.245104
- 24 C. H. Kim, H. S. Kim, H. Jeong, H. Jin and J. Yu, *Phys. Rev. Lett.*, 2012, **108**, 106401. DOI:10.1103/PhysRevLett.108.106401
- 25 K. Sun, W. V. Liu, A. Hemmerich and S. Das Sarma, *Nat. Phys.*, 2012, **8**, 67–70. DOI:10.1038/nphys2134
- 26 X. Wan, A. M. Turner, A. Vishwanath and S. Y. Savrasov, *Phys. Rev. B - Condens. Matter Mater. Phys.*, 2011, **83**, 205101. DOI:10.1103/PhysRevB.83.205101

- 27 S. Jia, S. Y. Xu and M. Z. Hasan, *Nat. Mater.*, 2016, **15**, 1140–1144. DOI:10.1038/nmat4787
- 28 X. Wan, A. Vishwanath and S. Y. Savrasov, *Phys. Rev. Lett.*, 2012, **108**, 146601. DOI:10.1103/PhysRevLett.108.146601
- 29 A. Kitaev, *Ann. Phys.*, 2006, **321**, 2–111. DOI:10.1016/j.aop.2005.10.005
- 30 G. Jackeli and G. Khaliullin, *Phys. Rev. Lett.*, 2009, **102**, 017205. DOI:10.1103/PhysRevLett.102.017205
- 31 Y. Zhou, P. A. Lee, T.-K. Ng and F.-C. Zhang, *Phys. Rev. Lett.*, 2008, **101**, 197201. DOI:10.1103/PhysRevLett.101.197201
- 32 M. Ge, T. F. Qi, O. B. Korneta, D. E. De Long, P. Schlottmann, W. P. Crummett and G. Cao, *Phys. Rev. B*, 2011, **84**, 100402. DOI:10.1103/PhysRevB.84.100402
- 33 S. Chikara, O. Korneta, W. P. Crummett, L. E. DeLong, P. Schlottmann and G. Cao, *Phys. Rev. B*, 2009, **80**, 140407. DOI:10.1103/PhysRevB.80.140407
- 34 Y. Okamoto, M. Nohara, H. Aruga-Katori and H. Takagi, *Phys. Rev. Lett.*, 2007, **99**, 137207. DOI:10.1103/PhysRevLett.99.137207
- 35 B. J. Kim, H. Jin, S. J. Moon, J. Y. Kim, B. G. Park, C. S. Leem, J. Yu, T. W. Noh, C. Kim, S. J. Oh, J. H. Park, V. Durairaj, G. Cao and E. Rotenberg, *Phys. Rev. Lett.*, 2008, **101**, 076402. DOI:10.1103/PhysRevLett.101.076402
- 36 S. J. Moon, H. Jin, K. W. Kim, W. S. Choi, Y. S. Lee, J. Yu, G. Cao, A. Sumi, H. Funakubo, C. Bernhard and T. W. Noh, *Phys. Rev. Lett.*, 2008, **101**, 226402. DOI:10.1103/PhysRevLett.101.226402
- 37 B. J. Kim, H. Ohsumi, T. Komesu, S. Sakai, T. Morita, H. Takagi and T. Arima, *Science*, 2009, **323**, 1329–1332. DOI:10.1126/science.1167106
- 38 X. Liu, T. Berlijn, W. G. Yin, W. Ku, A. Tselvik, Y. J. Kim, H. Gretarsson, Y. Singh, P. Gegenwart and J. P. Hill, *Phys. Rev. B - Condens. Matter Mater. Phys.*, 2011, **83**, 220403. DOI:10.1103/PhysRevB.83.220403
- 39 F. Ye, S. Chi, H. Cao, B. C. Chakoumakos, J. A. Fernandez-Baca, R. Custelcean, T. F. Qi, O. B. Korneta and G. Cao, *Phys. Rev. B*, 2012, **85**, 180403. DOI:10.1103/PhysRevB.85.180403
- 40 M. A. Laguna-Marco, D. Haskel, N. Souza-Neto, J. C. Lang, V. V. Krishnamurthy, S. Chikara, G. Cao and M. van Veenendaal, *Phys. Rev. Lett.*, 2010, **105**, 216407. DOI:10.1103/PhysRevLett.105.216407
- 41 G. Cao, J. E. Crow, R. P. Guertin, P. F. Henning, C. C. Homes, M. Strongin, D. N. Basov and E. Lochner, *Solid State Commun.*, 2000, **113**, 657–662. DOI:10.1016/S0038-1098(99)00532-3
- 42 G. Cao, X. N. Lin, S. Chikara, V. Durairaj and E. Elhami, *Phys. Rev. B - Condens. Matter Mater. Phys.*, 2004, **69**, 174418. DOI:10.1103/PhysRevB.69.174418
- 43 K. Maiti, R. S. Singh, V. R. R. Medicherla, S. Rayaprol and E. V. Sampathkumaran, *Phys. Rev. Lett.*, 2005, **95**, 6–9. DOI:10.1103/PhysRevLett.95.016404
- 44 G. Cao, Y. Xin, C. S. Alexander, J. E. Crow, P. Schlottmann, M. K. Crawford, R. L. Harlow and W. Marshall, *Phys. Rev. B - Condens. Matter Mater. Phys.*, 2002, **66**, 214412. DOI:10.1103/PhysRevB.66.214412
- 45 Y. Ping, G. Galli and W. A. Goddard, *J. Phys. Chem. C*, 2015, **119**, 11570–11577. DOI:10.1021/acs.jpcc.5b00861
- 46 J. Xu, T. Jarlborg and A. Freeman, *Phys. Rev. B*, 1989, **40**, 7939–7947. DOI:10.1103/PhysRevB.40.7939
- 47 J. S. de Almeida and R. Ahuja, *Phys. Rev. B*, 2006, **73**, 165102. DOI:10.1103/PhysRevB.73.165102
- 48 P. Mori-Sánchez, A. J. Cohen and W. Yang, *Phys. Rev. Lett.*, 2008, **100**, 146401. DOI:10.1103/PhysRevLett.100.146401
- 49 M. K. Y. Chan and G. Ceder, *Phys. Rev. Lett.*, 2010, **105**, 196403. DOI:10.1103/PhysRevLett.105.196403
- 50 W. Kohn, *Rev. Mod. Phys.*, 1999, **71**, 1253–1266. DOI:10.1103/RevModPhys.71.1253
- 51 F. Bechstedt, F. Fuchs and G. Kresse, *Phys. status solidi*, 2009, **246**, 1877–1892. DOI:10.1002/pssb.200945074
- 52 D. Bagayoko, *AIP Adv.*, 2014, **4**, 127104. DOI:10.1063/1.4903408
- 53 S. K. Panda, S. Bhowal, A. Delin, O. Eriksson and I. Dasgupta, *Phys. Rev. B*, 2014, **89**, 155102. DOI:10.1103/PhysRevB.89.155102
- 54 X. Xu, J. Jiang, W. J. Shi, V. Süß, C. Shekhar, S. C. Sun, Y. J. Chen, S.-K. Mo, C. Felser, B. H. Yan, H. F. Yang, Z. K. Liu, Y. Sun, L. X. Yang and Y. L. Chen, *Phys. Rev. B*, 2019, **99**, 195106. DOI:10.1103/PhysRevB.99.195106
- 55 J. N. Nelson, J. P. Ruf, Y. Lee, C. Zeledon, J. K. Kawasaki, S. Moser, C. Jozwiak, E. Rotenberg, A. Bostwick, D. G. Schlom, K. M. Shen and L. Moreschini, *Phys. Rev. Mater.*, 2019, **3**, 064205. DOI:10.1103/PhysRevMaterials.3.064205
- 56 H. Lee, J. Y. Kim, S. Y. Lee, J. A. Hong, N. Kim, J. Baik and Y. J. Hwang, *Sci. Rep.*, 2018, **8**, 16777. DOI:10.1038/s41598-018-35116-w
- 57 J. K. Kawasaki, C. H. Kim, J. N. Nelson, S. Crisp, C. J. Zollner, E. Biegenwald, J. T. Heron, C. J. Fennie, D. G. Schlom and K. M. Shen, *Phys. Rev. Lett.*, 2018, **121**, 176802. DOI:10.1103/PhysRevLett.121.176802
- 58 P. Kumar Das, J. Sławińska, I. Vobornik, J. Fujii, A. Regoutz, J. M. Kahn, D. O. Scanlon, B. J. Morgan, C. McGuinness, E. Plekhanov, D. Di Sante, Y.-S. Huang, R.-S. Chen, G. Rossi, S. Picozzi, W. R. Branford, G. Panaccione and D. J. Payne, *Phys. Rev. Mater.*, 2018, **2**, 65001. DOI:10.1103/PhysRevMaterials.2.065001
- 59 J. K. Kawasaki, D. Baek, H. Paik, H. P. Nair, L. F. Kourkoutis, D. G. Schlom and K. M. Shen, *Phys. Rev. Mater.*, 2018, **2**, 54206. DOI:10.1103/PhysRevMaterials.2.054206
- 60 E. W. Plummer, J. Shi, S.-J. Tang, E. Rotenberg and S. D. Kevan, *Prog. Surf. Sci.*, 2003, **74**, 251–268. DOI:10.1016/j.progsurf.2003.08.033
- 61 T. Chien, E. D. L. Rienks, M. F. Jensen, P. Hofmann and E. W. Plummer, *Phys. Rev. B*, 2009, **80**, 241416. DOI:10.1103/PhysRevB.80.241416
- 62 A. Eiguren, B. Hellsing, F. Reinert, G. Nicolay, E. V. Chulkov, V. M. Silkin, S. Hüfner and P. M. Echenique, *Phys. Rev. Lett.*, 2002, **88**, 066805. DOI:10.1103/PhysRevLett.88.066805
- 63 F. Reinert, G. Nicolay, S. Schmidt, D. Ehm and S. Hüfner, *Phys. Rev. B*, 2001, **63**, 115415. DOI:10.1103/PhysRevB.63.115415
- 64 T. Valla, A. V. Fedorov, P. D. Johnson, P. A. Glans, C. McGuinness, K. E. Smith, E. Y. Andrei and H. Berger, *Phys. Rev. Lett.*, 2004, **92**, 086401. DOI:10.1103/PhysRevLett.92.086401
- 65 V. Jovic, R. J. Koch, S. K. Panda, H. Berger, P. Bugnon, A. Magrez, K. E. Smith, S. Biermann, C. Jozwiak, A. Bostwick, E. Rotenberg and S. Moser, *Phys. Rev. B*, 2018, **98**, 241101. DOI:10.1103/PhysRevB.98.241101
- 66 N. Taira, M. Wakeshima and Y. Hinatsu, *J. Phys. Condens. Matter*, 2001, **13**, 5527–5533. DOI:10.1088/0953-8984/13/23/312
- 67 K. Matsuhira, M. Wakeshima, R. Nakanishi, T. Yamada, A. Nakamura, W. Kawano, S. Takagi and Y. Hinatsu, *J. Phys. Soc. Japan*, 2007, **76**, 043706. DOI:10.1143/JPSJ.76.043706
- 68 S. T. Bramwell, *Science*, 2001, **294**, 1495–1501. DOI:10.1126/science.1064761
- 69 J. S. Gardner, M. J. P. Gingras and J. E. Greedan, *Rev. Mod. Phys.*, 2010, **82**, 53–107. DOI: 10.1103/RevModPhys.82.53
- 70 D. Yanagishima and Y. Maeno, *J. Phys. Soc. Japan*, 2001, **70**, 2880–2883. DOI:10.1143/JPSJ.70.2880
- 71 S. Nakatsuji, Y. Maehara, Y. Maeno, T. Tayama, T. Sakakibara, J. Van Duijn, L. Balicas, J. N. Millican, R. T. MacAluso and J. Y. Chan, *Phys. Rev. Lett.*, 2006, **96**, 087204. DOI:10.1103/PhysRevLett.96.087204
- 72 Y. Maehara, S. Nakatsuji, Y. Maeno, T. Tayama, T. Sakakibara and S. Onoda, *Phys. Rev. Lett.*, 2007, **98**, 057203. DOI:10.1103/PhysRevLett.98.057203
- 73 K. Ueda, J. Fujioka and Y. Tokura, *Phys. Rev. B*, 2016, **93**, 245120. DOI:10.1103/PhysRevB.93.245120

- 74 T. Kondo, M. Nakayama, R. Chen, J. J. Ishikawa, E. G. Moon, T. Yamamoto, Y. Ota, W. Malaeb, H. Kanai, Y. Nakashima, Y. Ishida, R. Yoshida, H. Yamamoto, M. Matsunami, S. Kimura, N. Inami, K. Ono, H. Kumigashira, S. Nakatsuji, L. Balents and S. Shin, *Nat. Commun.*, 2015, **6**, 10042. DOI:10.1038/ncomms10042
- 75 K. Ueda, J. Fujioka, C. Terakura and Y. Tokura, *RAPID Commun. Phys. Rev. B*, 2015, **92**, 121110. DOI:10.1103/PhysRevB.92.121110
- 76 G. Chen and M. Hermele, *Phys. Rev. B*, 2012, **86**, 235129. DOI:10.1103/PhysRevB.86.235129
- 77 K. Ueda, J. Fujioka, B. J. Yang, J. Shiogai, A. Tsukazaki, S. Nakamura, S. Awaji, N. Nagaosa and Y. Tokura, *Phys. Rev. Lett.*, 2015, **115**, 056402. DOI:10.1103/PhysRevLett.115.056402
- 78 Z. Tian, Y. Kohama, T. Tomita, H. Ishizuka, T. H. Hsieh, J. J. Ishikawa, K. Kindo, L. Balents and S. Nakatsuji, *Nat. Phys.*, 2016, **12**, 134–138. DOI:10.1038/nphys3567
- 79 K. Ueda, T. Oh, B.-J. Yang, R. Kaneko, J. Fujioka, N. Nagaosa and Y. Tokura, *Nat. Commun.*, 2017, **8**, 15515. DOI:10.1038/ncomms15515
- 80 P. Goswami, B. Roy and S. Das Sarma, *Phys. Rev. B*, 2017, **95**, 85120. DOI:10.1103/PhysRevB.95.085120
- 81 T. Oh, H. Ishizuka and B.-J. Yang, *Phys. Rev. B*, 2018, **98**, 144409. DOI:10.1103/PhysRevB.98.144409
- 82 K. Ueda, H. Fukuda, R. Kaneko, J. Fujioka and Y. Tokura, *Phys. Rev. B*, 2020, **102**, 245131. DOI:10.1103/PhysRevB.102.245131
- 83 V. N. Antonov, L. V. Bekenov and D. A. Kukusta, *Phys. Rev. B*, 2020, **102**, 195134. DOI:10.1103/PhysRevB.102.195134
- 84 R. Kaneko, M.-T. Huebsch, S. Sakai, R. Arita, H. Shinaoka, K. Ueda, Y. Tokura and J. Fujioka, *Phys. Rev. B*, 2019, **99**, 161104. DOI:10.1103/PhysRevB.99.161104
- 85 B. J. Kennedy, *J. Solid State Chem.*, 1996, **123**, 14–20. DOI:10.1006/jssc.1996.0146
- 86 H. Okabe, M. Isobe, E. Takayama-Muromachi, A. Koda, S. Takeshita, M. Hiraishi, M. Miyazaki, R. Kadono, Y. Miyake and J. Akimitsu, *Phys. Rev. B - Condens. Matter Mater. Phys.*, 2011, **83**, 155118. DOI:10.1103/PhysRevB.83.155118
- 87 M. Uchida, Y. F. Nie, P. D. C. King, C. H. Kim, C. J. Fennie, D. G. Schlom and K. M. Shen, *Phys. Rev. B*, 2014, **90**, 075142. DOI:10.1103/PhysRevB.90.075142
- 88 P. Schütz, D. Di Sante, L. Dudy, J. Gabel, M. Stübinger, M. Kamp, Y. Huang, M. Capone, M. A. Husanu, V. N. Strocov, G. Sangiovanni, M. Sing and R. Claessen, *Phys. Rev. Lett.*, 2017, **119**, 256404. DOI:10.1103/PhysRevLett.119.256404
- 89 A. V. Powell and P. D. Battle, *J. Alloys Compd.*, 1993, **191**, 313–318. DOI:10.1016/0925-8388(93)90085-2
- 90 R. Lindsay, W. Strange, B. L. Chamberland and R. O. Moyer, *Solid State Commun.*, 1993, **86**, 759–763. DOI:10.1016/0038-1098(93)90186-Q
- 91 T. C. Kaspar, S. M. Heald, C. M. Wang, J. D. Bryan, T. Droubay, V. Shutthanandan, S. Thevuthasan, D. E. McCready, A. J. Kellock, D. R. Gamelin and S. A. Chambers, *Phys. Rev. Lett.*, 2005, **95**, 217203. DOI:10.1103/PhysRevLett.95.217203
- 92 D. Kim, J. Hong, Y. Ran Park and K. Joo Kim, *J. Phys. Condens. Matter*, 2009, **21**, 195405. DOI:10.1088/0953-8984/21/19/195405
- 93 A. K. Rumaiz, B. Ali, A. Ceylan, M. Boggs, T. Beebe and S. Ismat Shah, *Solid State Commun.*, 2007, **144**, 334–338. DOI:10.1016/j.ssc.2007.08.034
- 94 J. B. Litteer, B.-H. Chen, J. C. Fettinger, B. W. Eichhorn, H. L. Ju and R. L. Greene, *Inorg. Chem.*, 2000, **39**, 458–462. DOI:10.1021/ic990356f
- 95 O. Gourdon, M. Evain, S. Jobic, R. Brec, H. J. Koo, M. H. Whangbo, B. Corraze and O. Chauvet, *Inorg. Chem.*, 2001, **40**, 2898–2904. DOI:10.1021/ic001434y
- 96 J. G. Cheng, J. S. Zhou, J. A. Alonso, J. B. Goodenough, Y. Sui, K. Matsubayashi and Y. Uwatoko, *Phys. Rev. B - Condens. Matter Mater. Phys.*, 2009, **80**, 104430. DOI:10.1103/PhysRevB.80.104430
- 97 M. H. Whangbo and H. J. Koo, *Solid State Commun.*, 2001, **118**, 491–495. DOI:10.1016/S0038-1098(01)00166-1
- 98 K. Maiti, *Phys. Rev. B - Condens. Matter Mater. Phys.*, 2006, **73**, 115119. DOI:10.1103/PhysRevB.73.115119
- 99 W. Ju, G.-Q. Liu and Z. Yang, *Phys. Rev. B*, 2013, **87**, 075112. DOI:10.1103/PhysRevB.87.075112
- 100 R. Arita, J. Kune, A. V. Kozhevnikov, A. G. Eguiluz and M. Imada, *Phys. Rev. Lett.*, 2012, **108**, 086403. DOI:10.1103/PhysRevLett.108.086403
- 101 A. Yamasaki, H. Fujiwara, S. Tachibana, D. Iwasaki, Y. Higashino, C. Yoshimi, K. Nakagawa, Y. Nakatani, K. Yamagami, H. Aratani, O. Kirilmaz, M. Sing, R. Claessen, H. Watanabe, T. Shirakawa, S. Yunoki, A. Naitoh, K. Takase, J. Matsuno, H. Takagi, A. Sekiyama and Y. Saitoh, *Phys. Rev. B*, 2016, **94**, 115103. DOI:10.1103/PhysRevB.94.115103
- 102 K. Terashima, M. Sunagawa, H. Fujiwara, T. Fukura, M. Fujii, K. Okada, K. Horigane, K. Kobayashi, R. Horie, J. Akimitsu, E. Golias, D. Marchenko, A. Varykhalov, N. L. Saini, T. Wakita, Y. Muraoka and T. Yokoya, *RAPID Commun. Phys. Rev. B*, 2017, **96**, 041106. DOI:10.1103/PhysRevB.96.041106
- 103 A. Louat, B. Lenz, S. Biermann, C. Martins, F. Bertran, P. Le Fèvre, J. E. Rault, F. Bert and V. Brouet, *Phys. Rev. B*, 2019, **100**, 205135. DOI:10.1103/PhysRevB.100.205135
- 104 F. Ye, C. Hoffmann, W. Tian, H. Zhao and G. Cao, *Phys. Rev. B*, 2020, **102**, 115120. DOI:10.1103/PhysRevB.102.115120
- 105 S. Boseggia, H. C. Walker, J. Vale, R. Springell, Z. Feng, R. S. Perry, M. Moretti Sala, H. M. Rønnow, S. P. Collins and D. F. McMorrow, *J. Phys. Condens. Matter*, 2013, **25**, 422202. DOI:10.1088/0953-8984/25/42/422202
- 106 C. Liu, S.-Y. Xu, N. Alidoust, T.-R. Chang, H. Lin, C. Dhital, S. Khadka, M. Neupane, I. Belopolski, G. Landolt, H.-T. Jeng, R. S. Markiewicz, J. H. Dil, A. Bansil, S. D. Wilson and M. Z. Hasan, *Phys. Rev. B*, 2014, **90**, 45127. DOI:10.1103/PhysRevB.90.045127
- 107 A. de la Torre, S. McKeown Walker, F. Y. Bruno, S. Riccò, Z. Wang, I. Gutierrez Lezama, G. Scheerer, G. Giriat, D. Jaccard, C. Berthod, T. K. Kim, M. Hoesch, E. C. Hunter, R. S. Perry, A. Tamai and F. Baumberger, *Phys. Rev. Lett.*, 2015, **115**, 176402. DOI:10.1103/PhysRevLett.115.176402
- 108 V. Brouet, J. Mansart, L. Perfetti, C. Piovera, I. Vobornik, P. Le, F. Bertran, S. C. Riggs, M. C. Shapiro, P. Giraldo-Gallo and I. R. Fisher, *RAPID Commun. Phys. Rev. B*, 2015, **92**, 81117. DOI:10.1103/PhysRevB.92.081117
- 109 J. Kim, D. Casa, M. H. Upton, T. Gog, Y. J. Kim, J. F. Mitchell, M. Van Veenendaal, M. Daghofer, J. Van Den Brink, G. Khaliullin and B. J. Kim, *Phys. Rev. Lett.*, 2012, **108**, 177003. DOI:10.1103/PhysRevLett.108.177003
- 110 D. Pincini, J. G. Vale, C. Donnerer, A. De La Torre, E. C. Hunter, R. Perry, M. Moretti Sala, F. Baumberger and D. F. McMorrow, *Phys. Rev. B*, 2017, **96**, 075162. DOI:10.1103/PhysRevB.96.075162
- 111 J. Kim, A. H. Said, D. Casa, M. H. Upton, T. Gog, M. Daghofer, G. Jackeli, J. Van Den Brink, G. Khaliullin and B. J. Kim, *Phys. Rev. Lett.*, 2012, **109**, 157402. DOI:10.1103/PhysRevLett.109.157402
- 112 J. Liu, J.-H. Chu, C. R. Serrao, D. Yi, J. Koralek, C. Nelson, C. Frontera, D. Krieger, L. Horak, E. Arenholz, J. Orenstein, A. Vishwanath, X. Marti and R. Ramesh, 2013, 1–5. arXiv:1305.1732v1 [cond-mat.str-el]
- 113 P. E. Evans, T. Komesu, L. Zhang, D. F. Shao, A. J. Yost, S. Kumar, E. F. Schwier, K. Shimada, E. Y. Tsybal, X. Hong and P. A. Dowben, *AIP Adv.*, 2020, **10**, 045027. DOI:10.1063/1.5135941

- 114 D. J. Groenendijk, C. Autieri, J. Girovsky, M. C. Martinez-Velarte, N. Manca, G. Mattoni, A. M. R. V. L. Monteiro, N. Gauquelin, J. Verbeeck, A. F. Otte, M. Gabay, S. Picozzi and A. D. Caviglia, *Phys. Rev. Lett.*, 2017, **119**, 256403. DOI:10.1103/PhysRevLett.119.256403
- 115 L. Zhang, X. Jiang, X. Xu and X. Hong, *APL Mater.*, 2020, **8**, 051108. DOI:10.1063/5.0005330
- 116 G. Cao, J. Bolivar, S. McCall, J. E. Crow and R. P. Guertin, *Phys. Rev. B*, 1998, **57**, R11039–R11042. DOI:10.1103/PhysRevB.57.R11039
- 117 J. M. Carter, V. V. Shankar, M. A. Zeb and H. Y. Kee, *Phys. Rev. B - Condens. Matter Mater. Phys.*, 2012, **85**, 115105. DOI:10.1103/PhysRevB.85.115105
- 118 Y. Chen, Y. M. Lu and H. Y. Kee, *Nat. Commun.*, 2015, **6**, 6593. DOI:10.1038/ncomms7593.
- 119 B. M. Wojek, M. H. Berntsen, S. Boseggia, A. T. Boothroyd, D. Prabhakaran, D. F. McMorrow, H. M. Ronnow, J. Chang and O. Tjernberg, *J. Phys. Condens. Matter*, 2012, **24**, 415602. DOI:10.1088/0953-8984/24/41/415602
- 120 J. Matsuno, K. Ihara, S. Yamamura, H. Wadati, K. Ishii, V. V. Shankar, H. Y. Kee and H. Takagi, *Phys. Rev. Lett.*, 2015, **114**, 247209. DOI:10.1103/PhysRevLett.114.247209.
- 121 Y. K. Kim, O. Krupin, J. D. Denlinger, A. Bostwick, E. Rotenberg, Q. Zhao, J. F. Mitchell, J. W. Allen and B. J. Kim, *Science*, 2014, **345**, 187–190. DOI:10.1126/science.1251151
- 122 Y. Liu, L. Yu, X. Jia, J. Zhao, H. Weng, Y. Peng, C. Chen, Z. Xie, D. Mou, J. He, X. Liu, Y. Feng, H. Yi, L. Zhao, G. Liu, S. He, X. Dong, J. Zhang, Z. Xu, C. Chen, G. Cao, X. Dai, Z. Fang and X. J. Zhou, *Sci. Rep.*, 2015, **5**, 13036. DOI:10.1038/srep13036
- 123 Y. Cao, Q. Wang, J. A. Waugh, T. J. Reber, H. Li, X. Zhou, S. Parham, S. R. Park, N. C. Plumb, E. Rotenberg, A. Bostwick, J. D. Denlinger, T. Qi, M. A. Hermele, G. Cao and D. S. Dessau, *Nat. Commun.*, 2016, **7**, 11367. DOI:10.1038/ncomms11367
- 124 C. Martins, B. Lenz, L. Perfetti, V. Brouet, F. Bertran and S. Biermann, *Phys. Rev. Mater.*, 2018, **2**, 32001. DOI:10.1103/PhysRevMaterials.2.032001
- 125 J. Chaloupka, G. Jackeli and G. Khaliullin, *Phys. Rev. Lett.*, 2010, **105**, 027204. DOI:10.1103/PhysRevLett.105.027204
- 126 Y. Singh, S. Manni, J. Reuther, T. Berlijn, R. Thomale, W. Ku, S. Trebst and P. Gegenwart, *Phys. Rev. Lett.*, 2012, **108**, 127203. DOI:10.1103/PhysRevLett.108.127203
- 127 S. K. Choi, R. Coldea, A. N. Kolmogorov, T. Lancaster, I. I. Mazin, S. J. Blundell, P. G. Radaelli, Y. Singh, P. Gegenwart, K. R. Choi, S.-W. Cheong, P. J. Baker, C. Stock and J. Taylor, *Phys. Rev. Lett.*, 2012, **108**, 127204. DOI:10.1103/PhysRevLett.108.127204
- 128 Y. Singh and P. Gegenwart, *Phys. Rev. B - Condens. Matter Mater. Phys.*, 2010, **82**, 064412. DOI:10.1103/PhysRevB.82.064412
- 129 C. H. Sohn, H. S. Kim, T. F. Qi, D. W. Jeong, H. J. Park, H. K. Yoo, H. H. Kim, J. Y. Kim, T. D. Kang, D. Y. Cho, G. Cao, J. Yu, S. J. Moon and T. W. Noh, *Phys. Rev. B - Condens. Matter Mater. Phys.*, 2013, **88**, 085125. DOI:10.1103/PhysRevB.88.085125
- 130 N. Alidoust, C. Liu, S.-Y. Xu, I. Belopolski, T. Qi, M. Zeng, D. S. Sanchez, H. Zheng, G. Bian, M. Neupane, Y.-T. Liu, S. D. Wilson, H. Lin, A. Bansil, G. Cao and M. Z. Hasan, *Phys. Rev. B*, 2016, **93**, 245132. DOI:10.1103/PhysRevB.93.245132
- 131 P. A. Dowben, *Surf. Sci. Rep.*, 2000, **40**, 151–247. DOI:10.1016/S0167-5729(00)00010-8
- 132 Y. Li, K. Foyevtsova, H. O. Jeschke and R. Valentí, *RAPID Commun. Phys. Rev. B*, 2015, **91**, 161101. DOI:10.1103/PhysRevB.91.161101
- 133 H. Gretarsson, J. P. Clancy, X. Liu, J. P. Hill, E. Bozin, Y. Singh, S. Manni, P. Gegenwart, J. Kim, A. H. Said, D. Casa, T. Gog, M. H. Upton, H. S. Kim, J. Yu, V. M. Katukuri, L. Hozoi, J. Van Den Brink and Y. J. Kim, *Phys. Rev. Lett.*, 2013, **110**, 076402. DOI:10.1103/PhysRevLett.110.076402
- 134 J. Rodriguez, G. Lopez, F. Ramirez, N. P. Breznay, R. Kealhofer, V. Nagarajan, D. Latzke, S. Wilson, N. Marrufo, P. Santiago, J. Lara, A. Diego, E. Molina, D. Rosser, H. Tavassol, A. Lanzara, J. G. Analytis and C. Ojeda-Aristizabal, *Phys. Rev. B*, 2020, **101**, 235415. DOI:10.1103/PhysRevB.101.235415
- 135 R. Comin, G. Levy, B. Ludbrook, Z. H. Zhu, C. N. Veenstra, J. A. Rosen, Y. Singh, P. Gegenwart, D. Stricker, J. N. Hancock, D. Van Der Marel, I. S. Elfimov and A. Damascelli, *Phys. Rev. Lett.*, 2012, **109**, 266406. DOI:10.1103/PhysRevLett.109.266406
- 136 F. Lüpke, S. Manni, S. C. Erwin, I. I. Mazin, P. Gegenwart and M. Wenderoth, *Phys. Rev. B - Condens. Matter Mater. Phys.*, 2015, **91**, 041405. DOI:10.1103/PhysRevB.91.041405
- 137 L. Moreschini, I. Lo Vecchio, N. P. Breznay, S. Moser, S. Ulstrup, R. Koch, J. Wirjo, C. Jozwiak, K. S. Kim, E. Rotenberg, A. Bostwick, J. G. Analytis and A. Lanzara, *RAPID Commun. Phys. Rev. B*, 2017, **96**, 161116. DOI:10.1103/PhysRevB.96.161116
- 138 S. Hirai, M. D. Welch, F. Aguado and S. A. T. Redfern, *Zeitschrift für Krist.*, 2009, **224**, 345–350. DOI:10.1524/zkri.2009.1138
- 139 J. G. Cheng, J. S. Zhou, J. B. Goodenough, Y. Sui, Y. Ren and M. R. Suichomel, *Phys. Rev. B - Condens. Matter Mater. Phys.*, 2011, **83**, 064401. DOI:10.1103/PhysRevB.83.064401
- 140 A. Subedi, *RAPID Commun. Phys. Rev. B*, 2012, **85**, 020408. DOI:10.1103/PhysRevB.85.020408
- 141 J. Fujioka, R. Yamada, M. Kawamura, S. Sakai, M. Hirayama, R. Arita, T. Okawa, D. Hashizume, M. Hoshino and Y. Tokura, *Nat. Commun.*, 2019, **10**, 362. DOI:10.1038/s41467-018-08149-y
- 142 R. Yamada, J. Fujioka, M. Kawamura, S. Sakai, M. Hirayama, R. Arita, T. Okawa, D. Hashizume, M. Hoshino and Y. Tokura, *Phys. Rev. Lett.*, 2019, **123**, 216601. DOI:10.1103/PhysRevLett.123.216601
- 143 M. Masuko, J. Fujioka, M. Nakamura, M. Kawasaki and Y. Tokura, *APL Mater.*, 2019, **7**, 081115. DOI:10.1063/1.5109582
- 144 M. Wakeshima, N. Taira, Y. Hinatsu and Y. Ishii, *Solid State Commun.*, 2003, **125**, 311–315. DOI:10.1016/S0038-1098(02)00823-2
- 145 G. Cao, V. Durairaj, S. Chikara, S. Parkin and P. Schlottmann, *Phys. Rev. B - Condens. Matter Mater. Phys.*, 2007, **75**, 134402. DOI:10.1103/PhysRevB.75.134402
- 146 I. Franke, P. J. Baker, S. J. Blundell, T. Lancaster, W. Hayes, F. L. Pratt and G. Cao, *Phys. Rev. B - Condens. Matter Mater. Phys.*, 2011, **83**, 094416. DOI:10.1103/PhysRevB.83.094416
- 147 M. M. Sala, K. Ohgushi, A. Al-Zein, Y. Hirata, G. Monaco and M. Krisch, *Phys. Rev. Lett.*, 2014, **112**, 176402. DOI:10.1103/PhysRevLett.112.176402
- 148 S. W. Kim, C. Liu, H. J. Kim, J. H. Lee, Y. Yao, K. M. Ho and J. H. Cho, *Phys. Rev. Lett.*, 2015, **115**, 096401. DOI:10.1103/PhysRevLett.115.096401
- 149 K. Matsuhira, K. Nakamura, Y. Yasukuni, Y. Yoshimoto, D. Hirai and Z. Hiroi, *J. Phys. Soc. Japan*, 2018, **87**, 013703. DOI:10.7566/JPSJ.87.013703
- 150 H. Hanate, T. Hasegawa, S. Tsutsui, K. Nakamura, Y. Yoshimoto, N. Kishigami, S. Haneta and K. Matsuhira, *J. Phys. Soc. Japan*, 2020, **89**, 053601. DOI:10.7566/JPSJ.89.053601
- 151 T. Hasegawa, W. Yoshida, K. Nakamura, N. Ogita and K. Matsuhira, *J. Phys. Soc. Japan*, 2020, **89**, 054602. DOI:10.7566/JPSJ.89.054602
- 152 A. G. Petukhov, J. Niggemann, V. N. Smelyanskiy and V. V. Osipov, *J. Phys. Condens. Matter*, 2007, **19**, 315205. DOI:10.1088/0953-8984/19/31/315205
- 153 D. Takegami, D. Kasinathan, K. K. Wolff, S. G. Altendorf, C. F. Chang, K. Hofer, A. Melendez-Sans, Y. Utsumi, F. Meneghin, T. D. Ha, C. H. Yen, K. Chen, C. Y. Kuo, Y. F. Liao, K. D. Tsuei, R. Morrow, S. Wurmehl, B. Büchner, B. E. Prasad, M.

## ARTICLE

## Journal Name

- Jansen, A. C. Komarek, P. Hansmann and L. H. Tjeng, *Phys. Rev. B*, 2020, **102**, 045119. DOI:10.1103/PhysRevB.102.045119
- 154 G. Cao, A. Subedi, S. Calder, J. Q. Yan, J. Yi, Z. Gai, L. Poudel, D. J. Singh, M. D. Lumsden, A. D. Christianson, B. C. Sales and D. Mandrus, *Phys. Rev. B - Condens. Matter Mater. Phys.*, 2013, **87**, 155136. DOI:10.1103/PhysRevB.87.155136
- 155 T. Dey, A. Maljuk, D. V Efremov, O. Kataeva, S. Gass, C. G. F. Blum, F. Steckel, D. Gruner, T. Ritschel, A. U. B. Wolter, J. Geck, C. Hess, K. Koepernik, J. Van Den Brink, S. Wurmehl and B. Büchner, *Phys. Rev. B*, 2016, **93**, 014434. DOI:10.1103/PhysRevB.93.014434
- 156 M. P. Ghimire, L.-H. Wu and X. Hu, *Phys. Rev. B*, 2016, **93**, 134421. DOI:10.1103/PhysRevB.93.134421